




Research Article
Mutagenesis

Systems chemo-biology analysis of DNA damage response and cell cycle effects induced by coal exposure

Jose F. Torres-Ávila^{1,2} , Lyda Espitia-Pérez³, Diego Bonatto⁴, Fernanda Rabaioli da Silva⁵, Iuri Marques de Oliveira¹, Luís F.O. Silva⁶, Dione Silva Corrêa⁷, Johnny Ferraz Dias⁸, Juliana da Silva^{9,5} and João Antonio Pêgas Henriques^{1,10}

¹Universidade Federal do Rio Grande do Sul, Centro de Biotecnologia, Departamento de Biofísica, Porto Alegre, RS, Brazil.

²Universidad Simón Bolívar, Facultad de Ciencias Básicas y Biomédicas, Barranquilla, Colombia.

³Universidad del Sinú, Grupo de Investigación Biomédica y Biología Molecular, Montería, Córdoba, Colombia.

⁴Centro de Biotecnologia da Universidade Federal do Rio Grande do Sul, Departamento de Biologia Molecular e Biotecnologia, Porto Alegre, RS, Brazil.

⁵Universidade La Salle, Canoas, RS, Brazil.

⁶Universidad de la Costa, Civil and Environmental Department, Barranquilla, Colombia.

⁷Universidade Luterana do Brasil, Programa de Pós-Graduação em Genética e Toxicologia Aplicada, Centro de Pesquisa de Produtos e Desenvolvimento, Canoas, RS, Brazil.

⁸Universidade Federal do Rio Grande do Sul, Instituto de Física, Laboratório de Implantação de Íons, Porto Alegre, RS, Brazil.

⁹Universidade Luterana do Brasil, Laboratório de Toxicologia Genética, Canoas, RS, Brazil.

¹⁰Universidade de Caxias do Sul, Instituto de Biotecnologia, Laboratório de Genômica, Proteômica e Reparo de DNA, RS, Brazil.

Abstract

Cell cycle alterations are among the principle hallmarks of cancer. Consequently, the study of cell cycle regulators has emerged as an important topic in cancer research, particularly in relation to environmental exposure. Particulate matter and coal dust around coal mines have the potential to induce cell cycle alterations. Therefore, in the present study, we performed chemical analyses to identify the main compounds present in two mineral coal samples from Colombian mines and performed systems chemo-biology analysis to elucidate the interactions between these chemical compounds and proteins associated with the cell cycle. Our results highlight the role of oxidative stress generated by the exposure to the residues of coal extraction, such as major inorganic oxides (MIOs), inorganic elements (IEs) and polycyclic aromatic hydrocarbons (PAH) on DNA damage and alterations in the progression of the cell cycle (blockage and/or delay), as well as structural dysfunction in several proteins. In particular, IEs such as Cr, Ni, and S and PAHs such as benzo[a]pyrene may have influential roles in the regulation of the cell cycle through DNA damage and oxidative stress. In this process, cyclins, cyclin-dependent kinases, zinc finger proteins such as TP53, and protein kinases may play a central role.

Keywords: Coal, Colombia, cell cycle, systems chemo-biology.

Received: April 25, 2019; Accepted: April 06, 2020.

Introduction

One of the largest open-pit coal mines in the world is located in northern Colombia Huertas *et al.* (2012a). According to the 2015 BP Statistical Energy Survey, Colombia aimed to increase its coal production by 35% to 115,000 tons per year

by 2015 from 85,000 tons in 2011. Open-pit mines were forecast to account for almost 50% of this increase (BP, 2014). According to Chaulya (2004) and Huertas *et al.* (2012b), activities associated with coal extraction during surface coal mining release major air pollutants into the atmosphere as particulate matter (PM) and coal dust. These activities include: topsoil removal, drilling, blasting, overburden loading and unloading, coal transport over unpaved roads and wind erosion of exposed surfaces. In addition to the coal itself, PM and coal dust

Send correspondence to José F. Torres-Ávila. Universidad Simón Bolívar, Facultad de Ciencias Básicas y Biomédicas, Carrera 59 N° 59-92, Barranquilla, Colombia. E-mail: jtortes69@unisimonbolivar.edu.co.

around coal mines can also contain O, N, H, trace species, and several inorganic minerals. The trace species may include SiO₂, Cu, Al, Ni, Cd, B, Sb, Fe, Pb, and Zn (Huertas *et al.*, 2012a). In mining, excessive occupational exposure to metals is considered to be the leading cause of metal-related cancers (Gloscow, 2007). Additionally, in open-cast coal mines, coal is stored at elevated ambient temperatures, where combustion may lead to the emission of polycyclic aromatic hydrocarbons (PAHs) (Liu *et al.*, 2008), most of which exhibit mutagenic and carcinogenic properties (Celik *et al.*, 2007).

There is a growing body of evidence that links long-term exposure to coal mining residues with increased risks of cardiovascular mortality (Pope and Dockery, 2006; Brook *et al.*, 2010), premature mortality (Callén *et al.*, 2009) and cancer (Pope 3rd *et al.*, 2002, 2011). However, the mechanisms underlying the development of these adverse effects are poorly understood. In vitro toxicological studies have found that exposure to PM induces cell damage including genotoxicity (de Kok *et al.*, 2005; Billet *et al.*, 2008), cell death (Hsiao *et al.*, 2000; Alfaro-Moreno *et al.*, 2002), cell cycle alterations (Poma *et al.*, 2006) and the stimulation of pro-inflammatory cytokine production (Schins and Borm, 1999). Some of the mechanisms proposed for these effects include the occurrence of oxidative damage through the production of reactive oxygen species (ROS) (Valko *et al.*, 2006); the release of growth factors, such as TGF- β (Borm, 1997; Sambandam *et al.*, 2015), and reduced proliferation associated with cell cycle arrest in response to genotoxic stresses and structural dysfunction of proteins (Kochach *et al.*, 2008; Gualtieri *et al.*, 2011). Furthermore, a recent study (Espitia-Pérez *et al.*, 2018) revealed a highly significant correlation between PM_{2.5} levels around the coal mining areas of northern Colombia and incidences of mitotic arrest, centromere damage, kinetochore malfunction and disruption of the mitotic spindle in local populations.

It has been shown that oxidative stress can override the spindle checkpoint (D'Angiolella *et al.*, 2007), inducing microtubule depolymerization (Parker *et al.*, 2014) and alterations in the spindle structure (Choi *et al.*, 2007). This observation supports prior results showing that the organic components of PM_{2.5}, particularly PAHs, have deleterious effects on the cell cycle and cause DNA damage (Longhin *et al.*, 2013). DNA-integrity checkpoints G1/S and G2/M and metaphase–anaphase (M/A) transitions are particularly implicated in cell cycle delay (Branzei and Foiani, 2008).

Considering that one of the main characteristics of cancer is cell cycle alterations (Otto and Sicinski, 2017). The study of cell cycle regulators, particularly in terms of exposure to environmental stressors, has emerged as a pertinent avenue of research in cancer studies (Puente *et al.*, 2014). Populations are rarely exposed to single air pollutants; therefore, experimental investigations which have focused on single-pollutant effects do not accurately assess real-world exposure risks. Consequently, a multi-pollutant perspective should be the focus of air quality management, rather than adhering to a single-pollutant viewpoint (Huang *et al.*, 2012). Furthermore, although several recent studies have investigated the combined toxicity of complex mixtures of chemicals (Labranche *et al.*,

2012), detailed investigations into synergistic toxicity and the possible mechanisms involved in biological responses to complex exposures remain scarce (Ku *et al.*, 2017). Therefore, in the present study, we performed a chemical analysis of mineral coals from two different Colombian mines to identify the main compounds present. We then performed systems chemo-biology analyses to reveal the interactions between these compounds and proteins associated with the cell cycle, elucidating their underlying regulatory mechanisms.

Material and Methods

Coal sample collection

To construct a chemo-biology interactome network for the proteins associated with the cell cycle and the major chemical constituents present in the coal samples, we chemically characterized bituminous and sub-bituminous coal samples, each collected from a different open-pit mine in Colombia. The samples were collected from coalfaces at the 'El Cerrejón' (La Guajira, Colombia) and 'Guacamaya' (Puerto Libertador, Córdoba, Colombia) coal mines in December 2013 (Figure S1). Six random points at each mine were sampled; samples were then prepared as a homogeneous pool. Coals from El Cerrejón are typically bituminous with a volatile content of 37.4% and an ash content of 6.8% (dry basis) (Feng *et al.*, 2003). Coals from Guacamaya are sub-bituminous with a high S content (2.30% total S with 1.06% as pyritic, 1.10% as organic and 0.14% from sulfates) and high volatile content (Prada *et al.*, 2016). While detailed chemical characterizations of El Cerrejón coal have been reported elsewhere (Nathan *et al.*, 1999), other Colombian coals, such as those obtained from the Guacamaya mine, have not been sufficiently characterized.

Analytical methods

Chemical analysis of the coal samples included identification of the major inorganic oxides (MIOs) in the coal ashes, inorganic element (IE) determination and quantification of PAHs, described in detail below.

Analysis of MIOs in coal ashes

A fraction of bituminous and sub-bituminous coal samples were incinerated separately at 815°C. The resulting ashes were processed according to the methods described by Norrish and Hutton (1969). Finally, the detection of MIOs was performed using X-ray fluorescence spectrometry (XRF) in a Philips PW2400 spectrometer system equipped with SuperQ software.

IE measurements by particle-induced X-ray emission (PIXE) assay

The elemental composition of each coal sample was measured by the conventional in vacuo PIXE assay, as described by Johansson *et al.* (1995). Individual portions of each coal sample were homogenized using a mortar, pressed into pellets, and then placed in the reaction chamber (at ~ 10⁻⁵ mbar), in a 3-MV Tandemron accelerator equipped with an energy resolution of ~ 155 eV to 5.9 keV for obtaining the spec-

tra. The spectra were analyzed using GUPIXWIN software (Campbell *et al.*, 2010), and expressed in parts per million. Each sample was evaluated three times in independent replicates to obtain the mean and standard deviation.

Measurement and quantification of PAHs

The PAH contents of the coal samples were quantified using the HPLC-UV/Vis method, according to Sun *et al.* (1998) and Cavalcante *et al.* (2008). Briefly, 5 g of each coal sample was dried at 30 °C for 24 h (in duplicate) for later extraction. The extraction was performed by ultrasonication in 5 mL acetone/hexane (1:1, v/v) for 15 min. The filtrate was concentrated on a rotary evaporator and then further under a stream of nitrogen gas to ~2 mL. A clean glass column was used for adsorption chromatography. The concentrated extracts were fractionated using a 20 × 1.5-cm column containing pre-cleaned silica gel (20 h at 110 °C). The column was first eluted with 20 mL hexane/dichloromethane (9:1, v/v), then with 30 mL hexane/dichloromethane (4:1, v/v) and finally with 10 mL dichloromethane/methanol (9:1, v/v). The eluted volumes were reduced to 1 mL, and finally, each extract was injected into a HPLC-UV system. The chromatographic conditions were as follows: 5 µm Kromasil C18 reverse-phase column (250 × 4.6 mm); injection volume: 20 µL; mobile phase (A): acetonitrile; mobile phase (B): MilliQ water; gradient method: 0 min (1:1), 10 min (7:3), 20 min (8:2), 25 min (8:2), 28 min (1:1), 30 min (1:1) and $\lambda = 254$ nm. Analytical curves were created using external standardization for quantification. In our study, we detected 11 PAHs in the samples. The PAHs detected and their limits of detection were: naphthalene (1.7976 g L⁻¹), acenaphthylene (0.0041 g L⁻¹), phenanthrene (0.1758 g L⁻¹), anthracene (0.0339 g L⁻¹), fluoranthene (0.3787 g L⁻¹), benzo[a]anthracene (0.3411 g L⁻¹), benzo[b]fluoranthene (0.0691 g L⁻¹), dibenzo[a,h]anthracene (1.1110 g L⁻¹), benzo[k]fluoranthene (2.2221 g L⁻¹), indene[1,2,3-cd]pyrene (3.5788 g L⁻¹) and benzo[g,h,i]perylene (0.0005 g L⁻¹). All chromatographic measurements were performed in duplicate at ambient temperature.

Interactome data mining and design of the chemo-biology network

To design the interactome network among the main chemical substances present in the coal samples and their potential interactions with *Homo sapiens* proteins involved in the cell cycle, we used the STITCH search engine version 5.0 [<http://stitch.embl.de/>] and STRING 10.0 [http://string-db.org/newstring.cgi/show_input_page.pl/] (Snel *et al.*, 2000; Jensen *et al.*, 2008). A total of 36 chemical elements were detected in the chemical analysis of both coal samples using the XRF, PIXE, and HPLC/UV/Vis methods, and these were used for the exploration of networks within the STITCH metasearch engine. While STITCH allows visualization of the physical interactions between chemical elements and proteins, the STRING metasearch engine generates protein-protein interactions (PPIs) (Feltes *et al.*, 2013). Each chemical-protein interaction (CPI) and PPI has a confidence level between 0 and 1.0 (where 1.0 indicates the highest confidence). Parameters

used by the STITCH and STRING metasearch engines were as follows: all predictive methods were enabled except text mining; interactions: 50; degree of confidence: 0.7 and network depth: 1. The results were combined and analyzed using Cytoscape 3.4.0 (Shannon *et al.*, 2003) and the search engine GeneCards (Rebhan *et al.*, 1997; Safran *et al.*, 2010) using the default parameters.

The chemical elements not involved in interactions according to STITCH were excluded. Then, using Cytoscape 3.4.0., we created the interactome that fused the small CPI and PPI networks (not shown individually) that were generated by STITCH and STRING, respectively.

Centrality analysis

To evaluate the node degree, betweenness, and to identify the ‘central’ nodes (chemical compounds/proteins) in the interactome, a centrality analysis of the interactome was performed using CentiScaPe 2.1 in Cytoscape (Scardoni *et al.*, 2009).

Modular analysis of the major CPI-PPI network

In the interactome or CPI-PPI network, we analyzed clusters or highly connected regions that are indicative of functional protein complexes. These regions were identified using the Molecular Complex Detection application (MCODE) (Bader and Hogue, 2003; Scott, 2017). The MCODE application is included within the Cytoscape program and was used with the following parameters: loops; grade limit: 2; cluster expansion by a neighbor shell allowed; removal of a single connected node from the clusters; cut-off node density: 0.1; node score limit: 0.2; score: 2 and maximum network depth: 100.

Gene ontology (GO) analysis

The genetic ontology analysis was performed using the Biological Networks GO tool (BiNGO 3.0.3) (Maere *et al.*, 2005), which is an application installed in Cytoscape. The clusters obtained with MCODE were analyzed to determine the main bioprocesses associated with each cluster. The degree of functional enrichment was evaluated quantitatively using the hypergeometric distribution by group and category (p-value). The false discovery rate algorithm (Benjamini and Hochberg, 1995) was used to correct for multiple tests, as implemented in BiNGO with a significance of $p < 0.05$.

Comet assay

The alkaline comet assay was carried out according to Singh *et al.* (1988) and Tice *et al.* (2000) with several modifications for a high-throughput comet assay version, which allows the processing of multiple samples (Tice *et al.*, 2000). The high-throughput “96-mini gel format” is an 8x12 multi-array on GelBond® film (Lonza, Rockland Inc. ME, USA) (McNamee, 2000) described by Kiskinis *et al.* (2002). Briefly, 6×10^4 V79 cells per well were seeded in 12-well cell culture plates and incubated for 24 h; plates were subsequently treated with a 0.15 mg/mL coal dilution from either El Cerrejón or Guacamaya for 24 h. The negative control was incubated with DMEM medium (FBS free), and the positive control was treated with 150 µM H₂O₂ for 3 h. For semi-automated scor-

ing, stained cells were analyzed using an Olympus BX51 fluorescence microscope (Olympus, Japan) and examined at 40X magnification under a green filter (540 nm). We analyzed 100 randomly selected nuclei, 50 from each of the two replicate slides (Gutzkow *et al.*, 2013). % tail DNA was scored using the Comet Assay IV software (Perceptive Instruments, Haverhill, UK). The alkaline comet assay using the lesion-specific enzyme Formamidopyrimidine DNA glycosylase (FPG) (New England Biolabs, MA, USA) was used to detect oxidized purines (Collins, 2009). The protocol was used as previously described with minor modifications for the high-throughput comet assay (Kushwaha, 2011). FPG recognizes oxidized purines, specifically 8-oxo-guanine (Kushwaha, 2011). All experiments were performed in triplicate.

The normality of the data was evaluated using the Kolmogorov–Smirnov test, while the Student’s *t*-test was used to compare results of the comet assay with and without the FPG enzyme. $P \leq 0.05$ was considered statistically significant. All analyses were performed using the Graphpad PRISM statistical software (Graphpad Inc., San Diego, CA).

Results

Chemical characterization, interactome data mining and design of the chemo-biology network

The chemical characterizations of the El Cerrejón and Guacamaya coal samples are shown in Tables S1–S3. Chemical analysis by XRF revealed a similar oxide composition for each coal ash (Table S1). A total of 10 different oxides were identified. As expected, samples from El Cerrejón showed a bulk chemical composition containing several metal oxides in the order $\text{SiO}_2 > \text{Al}_2\text{O}_3 > \text{Fe}_2\text{O}_3 > \text{K}_2\text{O} > \text{MgO}$. Ashes from the sub-bituminous coal samples from Guacamaya showed higher concentrations of CaO, MgO, and SO_3 and lower concentrations of SiO_2 and Al_2O_3 than those reported in similar studies on bituminous and sub-bituminous coals (Blissett and Rowson, 2012).

As shown in Table S2, 15 IEs were identified by PIXE. Typically, bituminous samples from El Cerrejón showed higher concentrations of Si, Al, S, and Fe than those from the sub-bituminous samples of Guacamaya. Conversely, relatively high concentrations of Na, Ca, and Mg were present in the Guacamaya samples. Sr was detected only in the Guacamaya samples. Finally, concentration data for the 11 PAHs identified by HPLC/UV/Vis are shown in Table S3. For both samples, the most abundant PAHs detected were naphthalene, phenanthrene, anthracene, fluoranthene and benzo[a]anthracene. In general, however, higher concentrations of all PAHs were found in the El Cerrejón samples.

Chemical characterization of the bituminous and sub-bituminous coal samples revealed no significant differences in their chemical compositions. 36 compounds (i.e., 10 MIOs detected in coal ash, 15 IEs, and 11 PAHs) were used to construct the chemo-biology interactome. Once unconnected compounds were excluded, the remaining 24 protein-interacting compounds were used to generate 48 small CPI-PPI networks using the STRING and STITCH metasearch engines (Table

Table 1 - Chemical constituents of coal samples found in the major CPI-PPI network.

Compound	Classification	Chemical classification
Acenaphthene	Organic	Polycyclic Aromatic Hydrocarbon
Anthracene	Organic	Polycyclic Aromatic Hydrocarbon
Benzo(a)pyrene	Organic	Polycyclic Aromatic Hydrocarbon
Benzo(b)fluoranthene	Organic	Polycyclic Aromatic Hydrocarbon
Fluoranthene	Organic	Polycyclic Aromatic Hydrocarbon
Naphthalene	Organic	Polycyclic Aromatic Hydrocarbon
Phenanthrene	Organic	Polycyclic Aromatic Hydrocarbon
SiO_2	Inorganic	Oxide of silicon
TiO_2	Inorganic	Oxide of titanium
Fe_2O_3	Inorganic	Oxide of iron
Al	Inorganic	Metal
Ca	Inorganic	Alkaline earth metal
Cl	Inorganic	Halogen
Cr	Inorganic	Transition metal
Fe	Inorganic	Transition metal
K	Inorganic	Alkali metal
Mg	Inorganic	Alkaline earth metal
Mn	Inorganic	Transition metal
Na	Inorganic	Alkali metal
Ni	Inorganic	Transition metal
S	Inorganic	Non-metal
Sr	Inorganic	Alkaline earth metal
Ti	Inorganic	Transition metal
Zn	Inorganic	Transition metal

1). All the small networks were combined, resulting in a large CPI-PPI network with 2,057 nodes and 24,957 edges (Figure S2). This large CPI-PPI network was then analyzed using CentiScaPe 2.1 to identify the nodes (proteins) occupying central positions in the network architecture. In this context, nodes known as hub-bottlenecks (HBs) are the most important and combine hub (high degree) and bottleneck (high betweenness) characteristics according to Azevedo and Moreira-Filho (2015). Through centrality analysis, we observed three HB nodes (UBC, UBA52, and RPS27A) and 15 bottlenecks (HSP90AA1, CAD, SRC, JUN, MAPK14, APP, CREBBP, AKT1, K, Na, Ni, Mg, Fe, benzo[a]pyrene and Cr) (Figure 1 and Table S4).

To understand how coal chemical constituents interact with cell cycle processes, we identified the modules in the main CPI-PPI network using the MCODE program. From these analyses, we obtained eight significant modules related to cell cycle processes (Figures 2 - 9). Clusters 6 (Figure 2), 11 (Figure 3), 13 (Figure 4), and 14 (Figure 5) are associated with MIOs, IEs and PAHs; clusters 9 (Figure 6) and 12 (Figure 7) appear to be associated with IEs and PAHs; finally clusters 2 (Figure 8) and 4 (Figure 9) are associated with IEs only. The

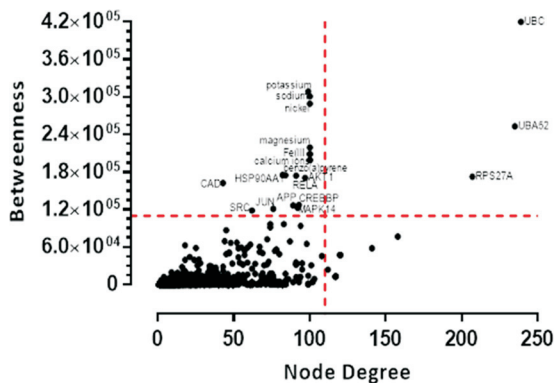


Figure 1 - Scatter plot of degree and betweenness values for all nodes. Hubs (high degree), bottlenecks (high betweenness), and nodes with high relative values in both parameters are identified.

analysis revealed 15 common proteins associated with different cell cycle processes.

The DNA damage induced by El Cerrejón and Guacamaya coal was determined by the modified alkaline high-throughput version of the comet assay and evaluated by the % tail DNA. The results of the comet assay showed statistically significant differences in relation to the negative control (NC) without enzyme ($P < 0.05$) and the % DNA tail increase. Additionally, the results of the modified comet assay showed a statistically significant difference when compared with the same sample group ($P < 0.05$) (Figure 10).

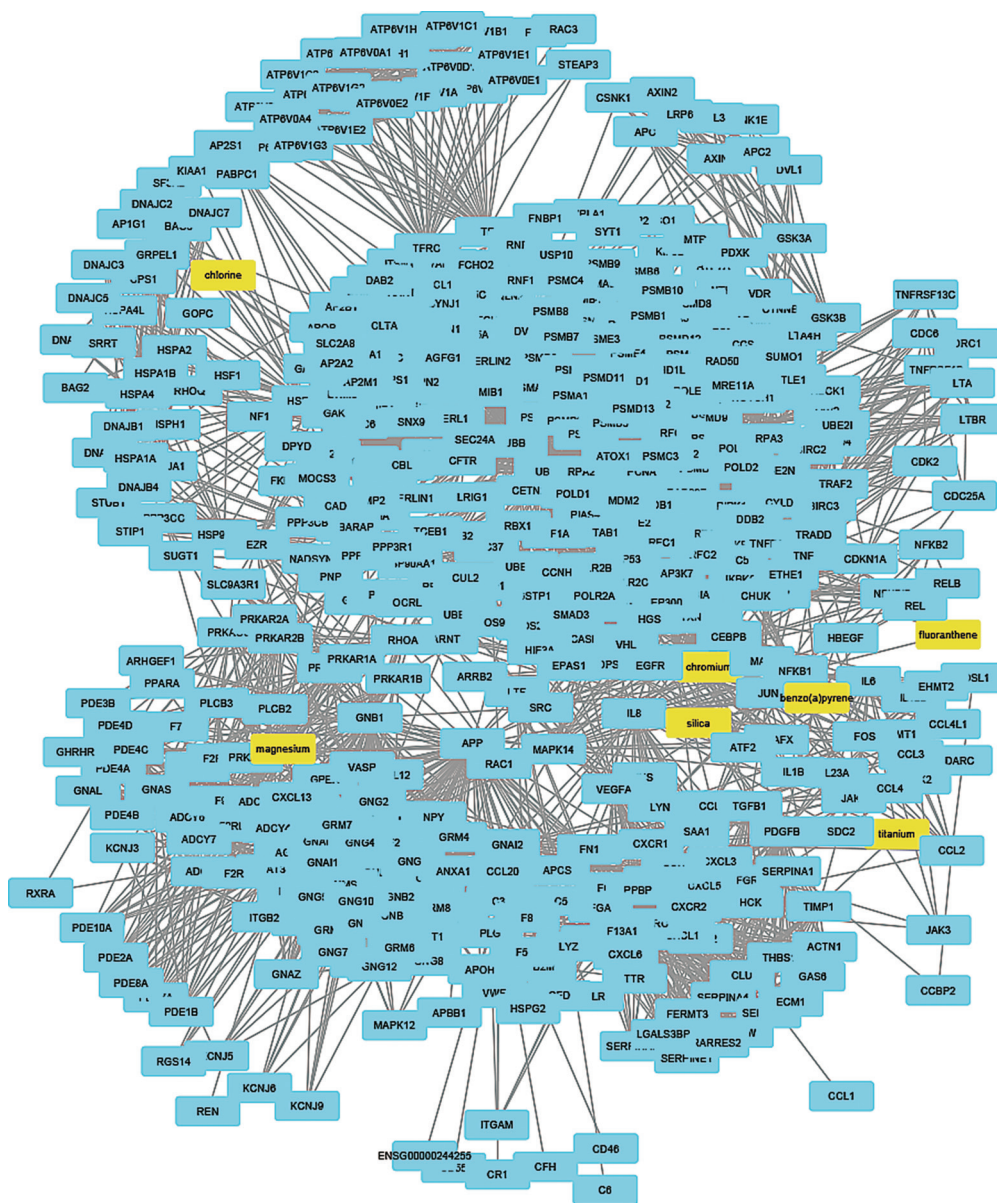


Figure 2 - Cluster analysis of the major CPI-PPI network showing the association of cluster 6 with MIOs, IEs, and PAHs (yellow). The cluster is composed of 487 nodes and 5,545 edges, with $C_i = 22,725$. The associated constituents are SiO_2 , Ti, Mg, Cr, Cl, fluoranthene, and benzo[a]pyrene.

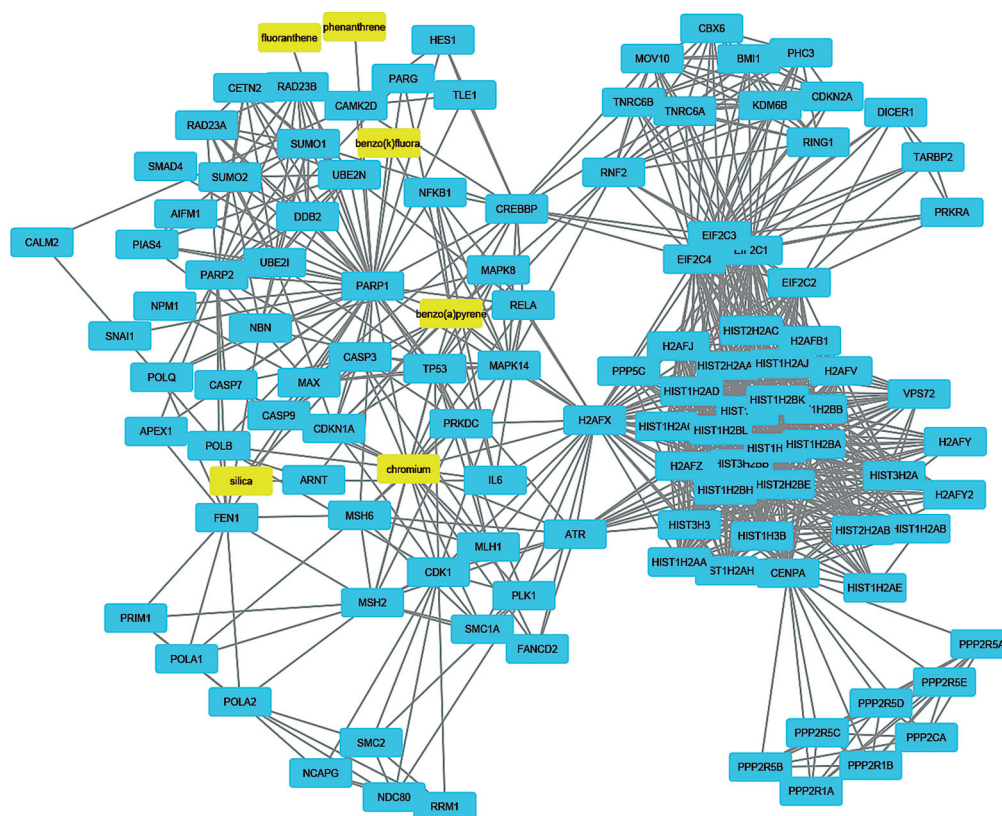


Figure 3 - Cluster analysis of the major CPI-PPI network showing the association of cluster 11 with MIOs, IEs, and PAHs (yellow). It is composed of 117 nodes and 867 edges, with $C_i = 14,695$. The associated constituents are SiO_2 , Cr, benzo[b]fluoranthene, fluoranthene, phenanthrene and benzo[a]pyrene.

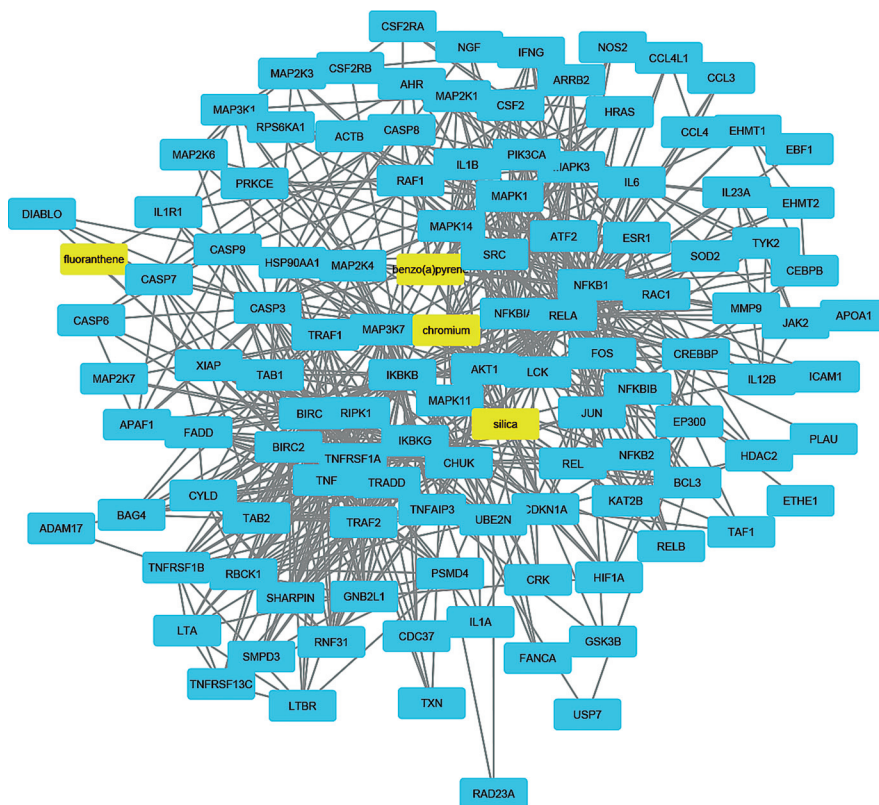


Figure 4 - Cluster analysis of the major CPI-PPI network showing the association of cluster 13 with MIOs, IEs, and PAHs (yellow). It is composed of 118 nodes and 732 edges, with $C_i = 12,303$. The associated constituents include SiO_2 , Cr, fluoranthene, and benzo[a]pyrene.

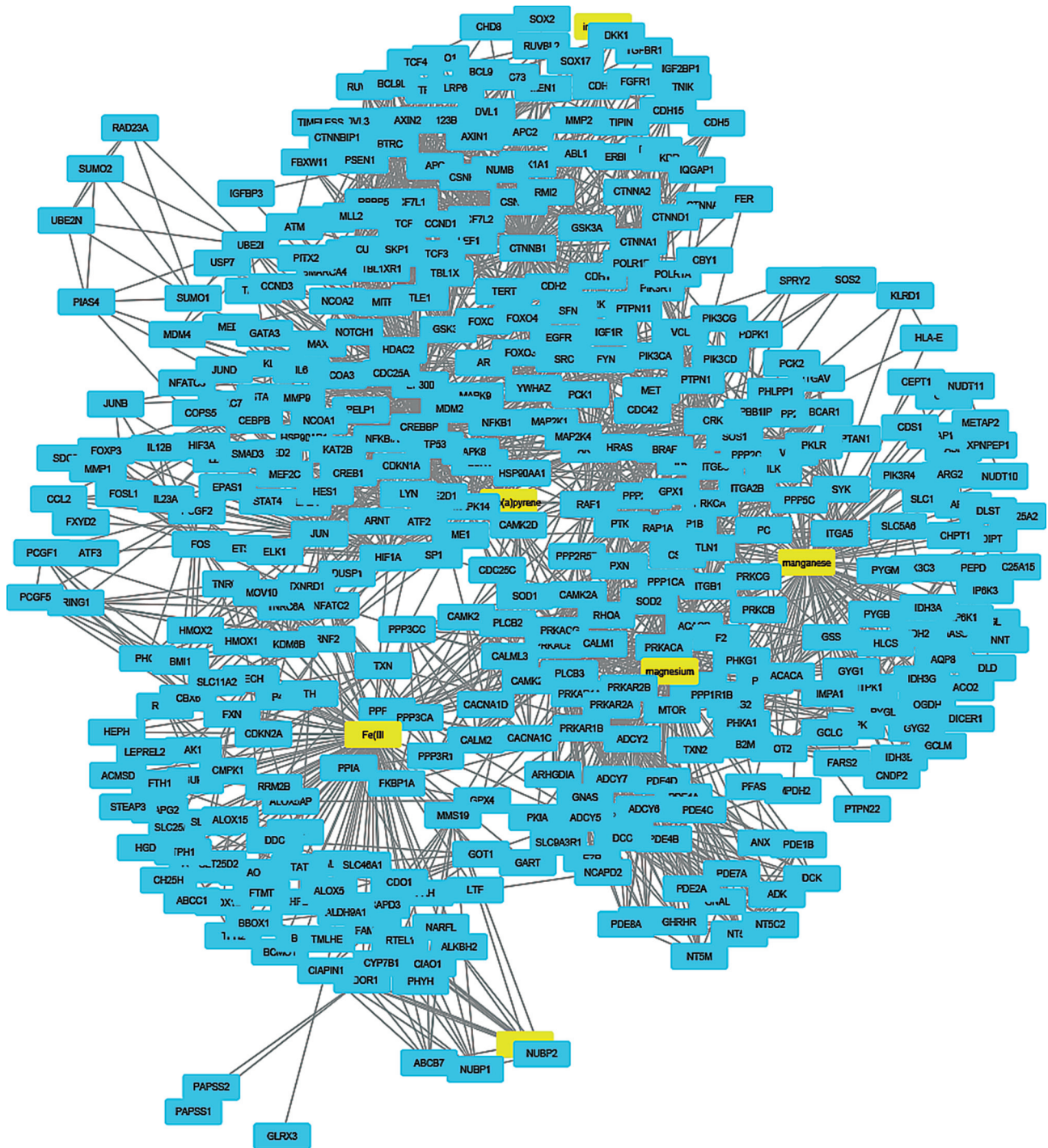


Figure 5 - Cluster analysis of the major CPI-PPI network showing the association of cluster 14 with MIOs, IEs, and PAHs (yellow). It is composed of 432 nodes and 2,520 edges, with $C_i = 1,164$. The associated constituents are S, Mn, Mg, Fe, Fe_2O_3 and benzo[a]pyrene.

Discussion

Ubiquitin (UBC) and two ubiquitin-coding genes (UBA52 and RPS27A) demonstrated the highest node degree and betweenness values, thus representing highly central proteins inside the network (Feltes *et al.*, 2013). UBC is a small 76-amino acid protein that is involved in several different pathways within the cell, including the clearing of dam-

aged/misfolded proteins during proteotoxic stress (Bianchi *et al.*, 2015). UBC genes are upregulated in response oxidative stress (Lee and Ryu, 2017), thereby increasing cellular UBC above threshold levels and conferring resistance to oxidative damage.

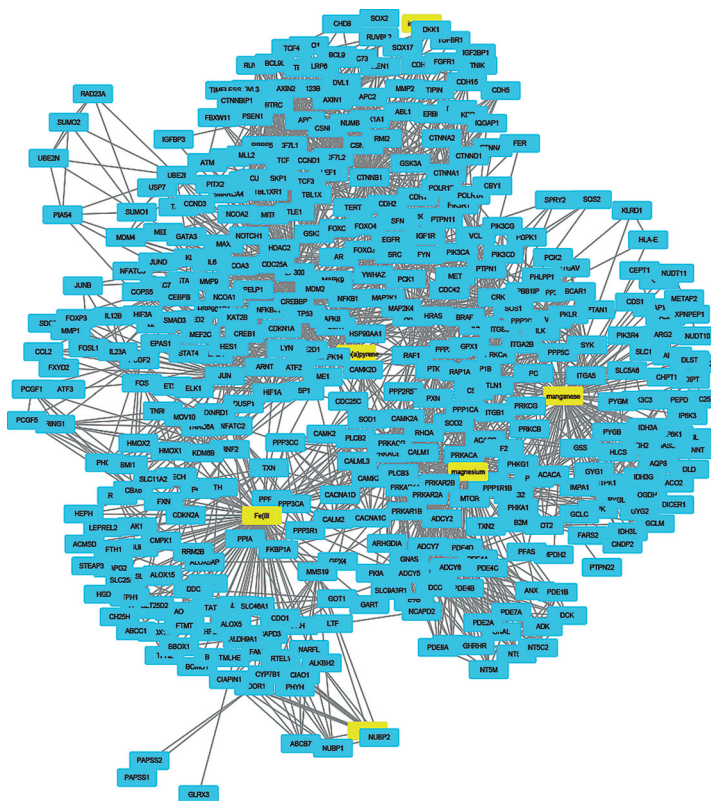


Figure 6 - Cluster analysis of the major CPI-PPI network showing the association of cluster 9 with IEs and PAHs (yellow). It is composed of 249 nodes and 2,180 edges, with $C_i = 17,44$. The associated compounds are S, Cr, Ti, and benzo[a]pyrene.

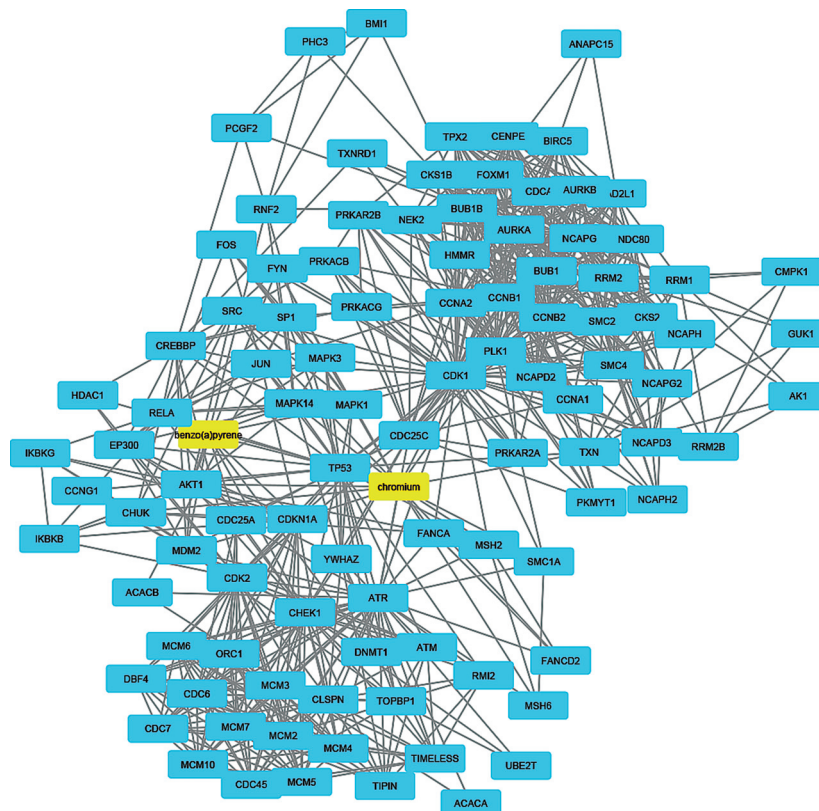


Figure 7 - Cluster analysis of the major CPI-PPI network showing the association of cluster 12 with IEs and PAHs (yellow). It is composed of 102 nodes and 741 edges, with $C_i = 14,388$. The associated compounds are Cr and benzo[a]pyrene.

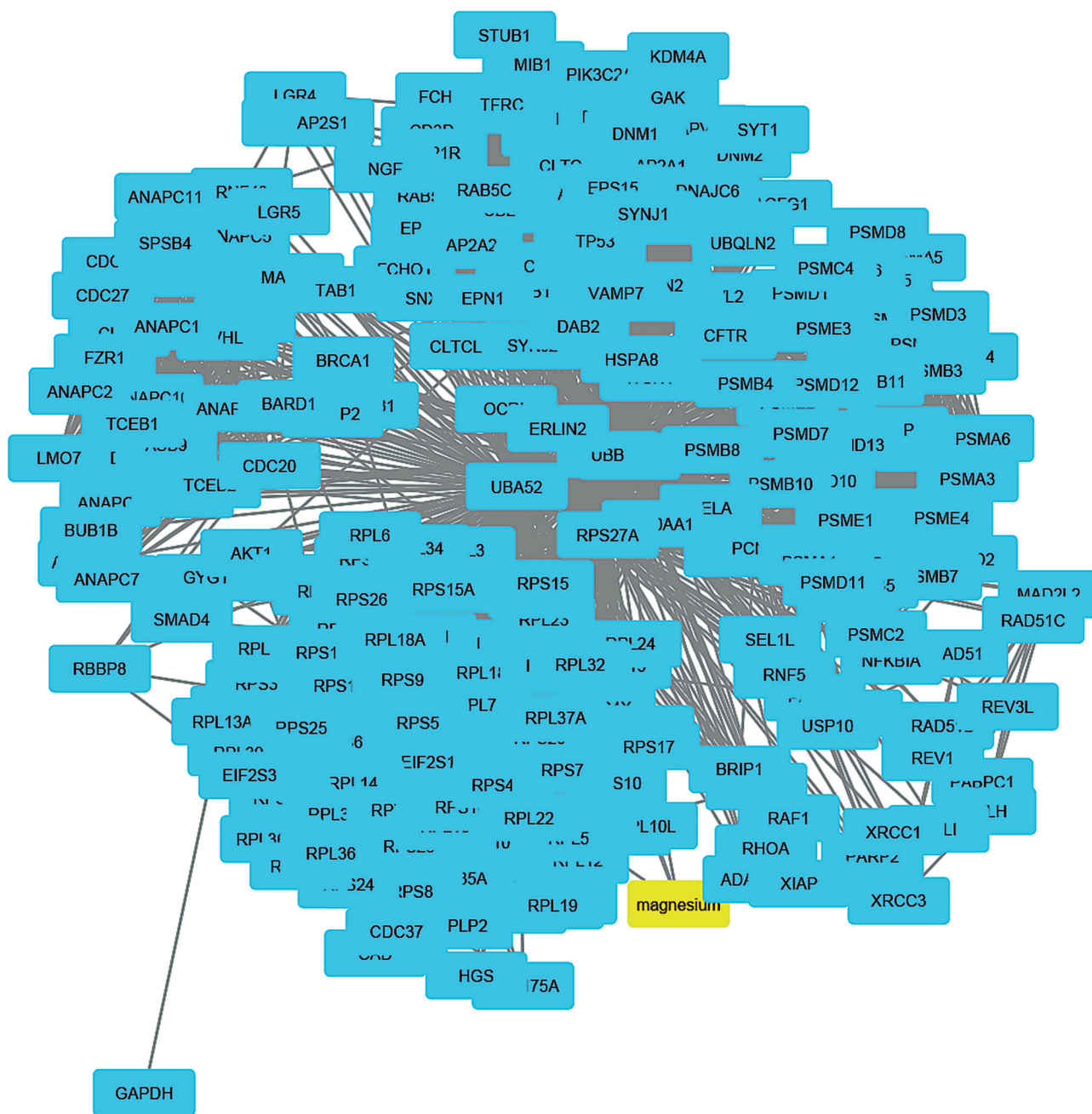


Figure 8 - Cluster analysis of the major CPI-PPI network showing association of cluster 2 with IEs (yellow). It is composed of 250 nodes and 5,976 edges, with $C_i = 47,618$, associated with Mg.

Systemic effects of MIOs, IEs and PAHs in the cell cycle and DNA damage

Tables 2–4 show the results of the GO analysis for each cluster and the cell cycle process categories. The main biological processes linked to clusters 6, 11, 13 and 14 included the following: (i) cell cycle process, (ii) mitotic cell cycle, (iii) cell cycle, (iv) cell cycle checkpoint, (v) regulation of cell cycle and (vi) cell cycle arrest (Table 2). Interestingly, DNA repair bioprocesses were found in this module only in co-occurrence with MIOs, IEs and PAHs. The particular combination of these compounds is associated with increased DNA damage in

cell systems *in vitro* (Leon-Mejia *et al.*, 2016) and human populations in coal mining environments (Leon-Mejia *et al.*, 2011). The primary mechanism proposed for these effects involves oxidative damage through the production of ROS (Valko *et al.*, 2006). In this regard, within the same module, proteins regulated by oxidative stress inside the cell were identified as bottlenecks (AKT, APP, JUN and CREBBP). While AKT has been reported to be regulated by oxidative stress for cell survival (Wang *et al.*, 2000), several studies have indicated that oxidative stress participates in events that enhance amyloidogenic APP processing in neurons (Lin and Beal,

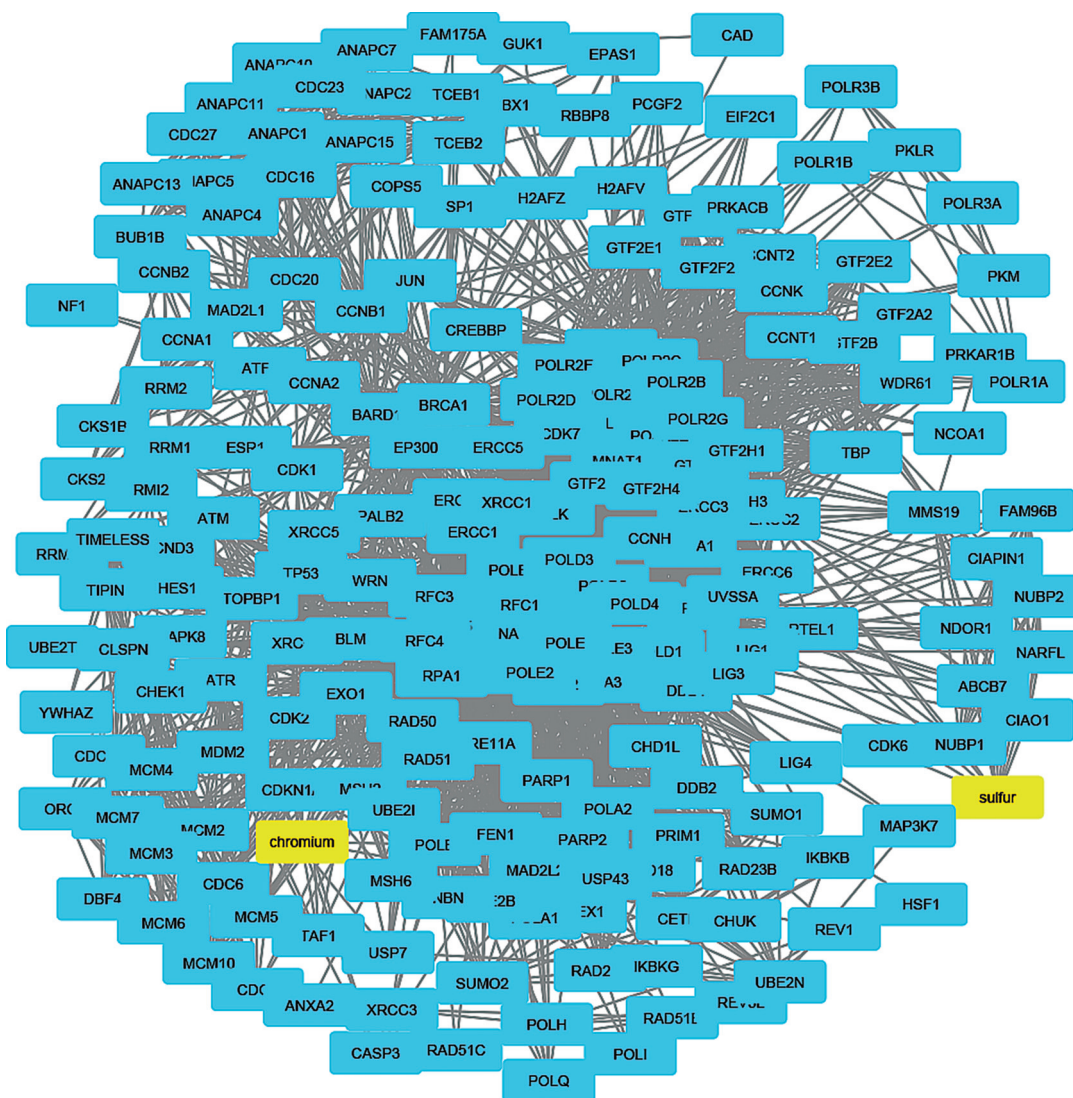


Figure 9 - Cluster analysis of the major CPI-PPI network showing association of cluster 4 with IEs (yellow). It is composed of 208 nodes and 3,134 edges, with $C_i = 2,999$, associated with Cr and S.

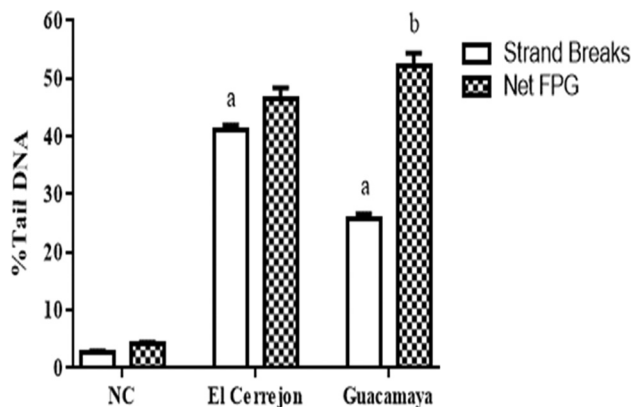


Figure 10 - Percent tail DNA in the alkaline comet assay (strand breaks in white) and oxidized purines (grid) in a modified comet assay with FPG in V79 cells under 24 h exposure with El Cerrejon and Guacamaya coal. a) Statistically significant differences in relation negative control (NC) without enzyme $P < 0.05$. b) Statistically significant differences in relation to the same sample group with an enzyme. The results are shown as the mean \pm SEM.

2006; Mouton-Liger *et al.*, 2012) and in events that affect cerebrovascular endothelial APP processing (Muche *et al.*, 2017). ROS-facilitated protein phosphorylation can also lead to kinase-mediated activation of transcription factors, such as the JUN group (Nathan and Cunningham-Bussel, 2013), affecting cell cycle progression by their ability to regulate the expression and function of cell cycle regulators such as cyclins (Schreiber *et al.*, 1999; Chiba *et al.*, 2017), and apoptosis (Meixner *et al.*, 2010). Together with JUN, CREBBP is also involved in cell division and cell proliferation, and it is upregulated by the oxidative stress response in retinoblastoma cells (Meixner *et al.*, 2010).

Oxidative stress can generate alterations in the progression of the cell cycle (blockage and/or delay), as well as structural dysfunction in several proteins. DNA-integrity checkpoints G1/S and G2/M, and M/A transitions determine cell cycle delays (Rieder, 2011) depending on the cyclin-dependent kinase (Cdk)/cyclin system, such as Cdk1/cyclin B1, which drives the progression from G2 to the mitotic phase

Table 2 - Major cell cycle bioprocesses in clusters 6, 11, 13 and 14 associated with MIOs, IEs and PAHs.

GO ID	p-value	corr p-value	k*	n [#]	Description	Genes in test set
22402	1,64E-22	9,74E-21	77	582	cell cycle process	APP CDKN1A CETN2 CLTC UBE2D1 PSMD8 PSMD9 PPP3CA PSMD7 PSMD4 PSMD2 PSMD3 PSMD1 AKT1 IL12B NBN POLE APC2 H2AFX CDC25A DNM2 PSMA5 PSMA6 DNAJC2 PSMA3 ADAM17 PSMA4 PSMA1 PSME3 PSME1 PSME2 TP53 PSMD10 PSMD12 PSMD11 RGS14 PSMD13 CUL2 THBS1 EGFR PSMB10 PSMB6 PSMB7 PSMB4 C6 PSMB5 PSMB2 PSMB3 POLD1 PSMB1 CLTCL1 APBB1 UBE2I TGFB1 SMAD3 VDR RPA1 MRE11A CDC6 HSPA2 PSMB8 MAPK12 PSMB9 PPP5C RAD50 PSMC6 PSMC3 APC IL8 PSMC4 PSMC1 PSMC2 CDK2 MDM2 CTNNB1 CALR SUGT1
278	9,54E-21	5,08E-19	60	380	mitotic cell cycle	APP CDKN1A CETN2 CLTC UBE2D1 PSMD8 PSMD9 PPP3CA PSMD7 PSMD4 PSMD2 PSMD3 PSMD1 AKT1 POLE APC2 CDC25A DNM2 PSMA5 PSMA6 DNAJC2 PSMA3 ADAM17 PSMA4 PSMA1 PSME3 PSME1 PSME2 PSMD10 PSMD12 PSMD11 RGS14 PSMD13 CUL2 EGFR PSMB10 PSMB6 PSMB7 PSMB4 C6 PSMB5 PSMB2 PSMB3 POLD1 PSMB1 CLTCL1 UBE2I CDC6 PSMB8 PSMB9 PPP5C PSMC6 PSMC3 APC PSMC4 PSMC1 PSMC2 CDK2 MDM2 SUGT1
7049	3,12E-18	1,43E-16	84	794	cell cycle	APP CDKN1A STEAP3 CCNH CETN2 CLTC UBE2D1 PSMD8 PSMD9 PPP3CA PSMD7 PSMD4 PSMD2 PSMD3 PSMD1 AKT1 IL12B EP300 NBN POLE APC2 ANXA1 H2AFX CDC25A DNM2 PSMA5 GAK PSMA6 DNAJC2 PSMA3 ADAM17 PSMA4 PSMA1 PSME3 PSME1 PSME2 TP53 PSMD10 PSMD12 PSMD11 RGS14 PSMD13 CUL2 THBS1 EGFR PSMB10 PSMB6 PSMB7 PSMB4 C6 PSMB5 PSMB2 PSMB3 POLD1 PSMB1 CLTCL1 APBB1 UBE2I TGFB1 SMAD3 VDR RPA1 MRE11A CDC6 HSPA2 PSMB8 MAPK12 PSMB9 CYLD PPP5C RAD50 PSMC6 PSMC3 APC IL8 PSMC4 PSMC1 PSMC2 CDK2 MDM2 CTNNB1 REN CALR SUGT1
22402	4,62E-06	1,46E-04	22	582	cell cycle process	CDKN1A NPM1 UBE2I CDKN2A CETN2 PLK1 H2AFX NCAPG SMC1A MLH1 CENPA NDC80 SMC2 MSH6 PPP2CA POLA1 PPP5C MSH2 FANCD2 CDK1 NBN TP53
75	5,61E-06	1,73E-04	11	107	cell cycle checkpoint	CDKN1A MSH2 CDKN2A PLK1 H2AFX CDK1 NBN PPP2R5C SMC1A TP53 ATR
6281	7,00E-12	4,71E-10	22	298	DNA repair	POLQ FEN1 PARP1 PRKDC PARP2 H2AFX RAD23A SMC1A MLH1 RAD23B DDB2 MSH6 POLB POLA1 MSH2 SUMO1 FANCD2 APEX1 UBE2N NBN TP53 ATR
51726	1,37E-05	1,78E-04	19	446	regulation of cell cycle	MAP2K1 JUN CREBBP CDKN1A HDAC2 NGF TNF CYLD KAT2B IL1A ADAM17 IFNG CDC37 CASP3 IL1B IL12B AKT1 HRAS MAP2K6
51726	5,25E-11	1,98E-09	48	447	regulation of cell cycle	CDS1 CDKN1A HDAC2 TRRAP HDAC1 CITED2 CUL1 ILK FOXO4 ETS1 EGFR SOX2 CCND3 CCND1 CDH1 AKT1 IL12B SFN PRKACA BTRC JUNB HRAS MEN1 APC2 TCF7L2 JUN CREBBP MAP2K1 TIPIN SMAD3 CDKN2A GSS INSR PTPN11 CDC25C CDC25A SMARCA4 FOSL1 KAT2B COPS5 APC PKIA MDM2 TIMELESS ATM TCF4 TCF3 TP53
22402	9,37E-06	1,83E-04	46	583	cell cycle process	CAMK2B CDKN1A NCAPG2 CUL1 UBE2D1 ILK FOXO4 EGFR SOX2 PPP2CA PPP3CA CCND1 CDH1 RUVBL1 ABL1 AKT1 IL12B BTRC HRAS MEN1 SKP1 APC2 TCF7L2 MAP2K1 TIPIN UBE2I SMAD3 CSNK1A1 CDKN2A GSS CDC25C CDC25A KAT2B PPP5C APC MDM2 TIMELESS CTNNB1 NCAPD2 MDM4 ATM TCF4 NCAPD3 TCF3 TP53 TAF1
7049	2,41E-05	4,31E-04	55	795	cell cycle	CDKN1A STEAP3 NCAPG2 UBE2D1 ILK CDC73 SOX2 PPP3CA CCND1 CDH1 RUVBL1 AKT1 IL12B EP300 BTRC HRAS MEN1 SKP1 APC2 MAP2K1 TIPIN ANXA1 DUSP1 FBXW11 CDC25C CDC25A KAT2B TIMELESS TP53 CDS1 CAMK2B CUL1 FOXO4 EGFR RNF2 PPP2CA ABL1 TCF7L2 UBE2I SMAD3 CSNK1A1 CDKN2A GSS PPP1CA PPP5C APC MDM2 CTNNB1 NCAPD2 MDM4 ATM TCF4 NCAPD3 TCF3 TAF1
7050	2,63E-05	4,64E-04	18	109	cell cycle arrest	TCF7L2 CDKN1A MAP2K1 SMAD3 CDKN2A GSS CUL1 ILK FOXO4 SOX2 KAT2B APC IL12B ATM TCF4 TP53 HRAS MEN1

#: total number of nodes in the gene ontology (GO) annotation; *: number of nodes related to a given GO in the network.

(Pearce and Humphrey, 2001). The protein kinases ataxia-telangiectasia mutated (ATM) and ATM and Rad3-related (ATR) promote DNA damage response and stimulate the checkpoint protein kinases Chk1/2, that can influence cell cycle arrest. CDK1 and other important proteins related to cell

cycle checkpoints (e.g. CDC25C and CDC25A), and DNA damage, were found to be the critical proteins inside this cluster. Oxidative stress often induces cell cycle arrest (Klein and Ackerman, 2003; Pyo *et al.*, 2013), in part through the degra-

duction of the CDC25C protein through a Chk1 protein kinase-dependent pathway (Savitsky and Finkel, 2002).

Cell cycle arrest associated with complex mixtures of PAHs, metals, and other organic compounds upon exposure to coal mining residues has been observed *in vitro* (Tucker and Ong, 1985) and *in vivo* (Espitia-Perez *et al.*, 2018). More recently, exposure to benzo[a]pyrene (also present in the cluster) has been reported to induce cell cycle arrest and apoptosis in human choriocarcinoma cancer cells through the generation of ROS (Kim *et al.*, 2017).

Systemic effects of IEs and PAHs in the cell cycle

As shown in Table 3, the GO analysis of clusters 9 and 12 revealed 14 main process annotations associated with the cell cycle and particularly Cr and benzo[a]pyrene. The main biological processes found in these clusters included the following: i) regulation of mitotic cell cycle, ii) cell cycle checkpoint and iii) the interphase of mitotic cell cycle. Several reports have demonstrated that more-than-additive mortality is common for IE/PAH mixtures. The PAH toxicity in individual aspects suggests that they modify the accumulation of IEs and improve element-derived reactive ROS. Redox-active elements (e.g., Cu and Ni) are also capable of enhancing the redox cycling of PAHs (Gauthier *et al.*, 2015). Several reports have implicated IEs as modifiers of P450 function and regulation, which implies that such elements could alter P450-mediated PAH mutagenicity and carcinogenicity (Peng *et al.*, 2015). Cr is typically used in coal mining processes (Pandey *et al.*, 2014) and is particularly associated with the fine fractions of PM (Kothai *et al.*, 2009). The genotoxic effects of Cr are predominantly the formation of oxidative adducts and apurinic/apyrimidinic lesions, eventually resulting in DNA breakage (Vasylykiv *et al.*, 2010). Additionally, Cr(VI) has been shown to be aneugenic, as revealed by both chromosome assays and centromere-positive micronuclei assays (Wise and Wise, 2010). However, the combined toxicity of Cr and benzo[a]pyrene has rarely been studied.

Interestingly, *in vitro* cell cycle analysis has demonstrated that mixtures of benzo[a]pyrene and metals reduce the cell population in the G1 phase and increase cell arrest or accumulation in the G2/M phase (Muthusamy *et al.*, 2018). Once more, the mechanisms suggested include oxidative stress (Fischer *et al.*, 2005), DNA repair alteration (Tran *et al.*, 2002), and suppressor protein TP53 inhibition (Chiang and Tsou, 2009). Particularly, *in vitro* exposure to a combination of benzo[a]pyrene with As, Cr and Pb increases the ROS-mediated oxidative stress in HepG2 cells (Muthusamy *et al.*, 2018). In this regard, within the same module, proteins regulated by oxidative stress and DNA damage inside the cell were also identified as bottlenecks (AKT1, JUN, and CREBBP) together with benzo[a]pyrene. Other trace species found in our IE analysis, such as SiO₂, have also been found to cause DNA damage, oxidative stress, cell cycle arrest at the G2/M checkpoint and apoptosis synergistically in co-exposure with benzo[a]pyrene (Asweto *et al.*, 2017).

Table 3 - Major cell cycle bioprocesses in clusters 9 and 12 associated with IEs and PAHs.

GO ID	p-value	corr p-	k*	n [#]	Description	Genes in test set
22402	2,71E-34	3,52E-31	67	582	cell cycle process	UBE2D BUB1B CDC20 PPP3CA CDC23 EXO1 CHEK1 CDC27 IL12B AKT1 NEK2 NBN HRAS TIPIN ANAPC7 H2AF X CDC25C RAD51B MSH6 CCNA2 CCNA1 RAD51 C MSH2 IFNG CKS2 TIMELESS ANAPC4 BIRC5 ANAPC5 TP53 ANAPC1 ANAPC2 ANAPC13 BLM CUL5 CUL2 NCAPG C C A8 PKMYT1 CENPA THBS1 ANAPC10 EGFR AURKB A NAPC11 AURKA CCNB2 CCNB1 FZR1 BARD1 UBE2I TGFBI PLK1 MRE11A CDC6 MLH1 NDC80 TPX2 CENPE RAD50 RAD51 CDC16 CDK2 CDK1 ATM MAD2L1
7049	3,93E-33	3,40E-30	75	794	cell cycle	UBE2D BUB1B FOXO1 CKS1B CDC20 PPP3CA CDC23 EXO1 CHEK1 CDC27 IL12B AKT1 NEK2 NBN HRAS TIPIN ANAPC7 H2AF X CDC25C RAD51B MSH6 CCNA2 CCNA1 RAD51 C MSH2 IFNG CKS2 TIMELESS ANAPC4 BIRC5 ANAPC5 TP53 ANAPC1 ANAPC2 ANAPC13 BLM CUL5 CUL2 NCAPG C C A8 PKMYT1 CENPA THBS1 ANAPC10 EGFR AURKB AURKA ANAPC11 AURKA CCNB2 CCNB1 FZR1 BARD1 UBE2I TGFBI PLK1 MRE11A CDC6 MLH1 NDC80 TPX2 CENPE RAD50 RAD51 CDC16 CDK2 CDK1 ATM MAD2L1
22403	2,04E-31	1,06E-28	57	435	cell cycle phase	BUB1B CDC20 PPP3CA CDC23 EXO1 CHEK1 CDC27 AKT1 NEK2 NBN TIPIN ANAPC7 H2AF X CDC25C RAD51B MSH6 CCNA2 CCNA1 RAD51 C CKS2 TIMELESS ANAPC4 BIRC5 ANAPC5 ANAPC1 ANAPC2 ANAPC13 BLM CUL5 C UL2 NCAPG C C A8 PKMYT1 ANAPC10 EGFR AURKB ANAPC11 AURKA CCNB2 CCNB1 FZR1 BARD1 UBE2I TGFBI PLK1 MRE11A CDC6 MLH1 NDC80 TPX2 CENPE RAD50 RAD51 CDC16 CDK2 CDK1 ATM MAD2L1
51726	1,03E-27	3,84E-25	54	446	regulation of cell cycle	BUB1B FOXO1 CKS1B CDC23 CHEK1 IL12B AKT1 NEK2 NBN PRKACA HRAS TIPIN H2AF X CDC25C CCNA2 MSH6 IFNG CDC37 CKS2 TIMELESS BIRC5 TP53 ANAPC2 BLM CUL5 CUL2 PKMYT1 THBS1 ANAPC10 EGFR BIRP1 CCNB1 FZR1 CDC45 IRBBP8 C LSPN BUB1 BARD1 JUN CREBBP TGFBI PLK1 MRE11A CDC6 TPX2 CENPE COP5 CDC16 FAM175A CDK2 CDK1 ATM ATR MAD2L1

Table 3 - cont.

278	6,00E-23	8,21E-21	46	380	mitotic cell cycle	ANAPC13 BLM CUL5 CUL2 NCAPG CDA8 UBE2D1 BUB1 IPKMYT1 CENPA ANAPC10 EGFR AURKB ANAPC11 AURKA CDC20 PPP3CA CCNB2 CCNB1 FZR1 CDC23 CDC27 AKT1 NEK2 BUB1 TIPIN UBE2J ANAPC7 PLK1 CDC6 CDC25 NDC80 CCNA2 TPX2 CENPE CCNA1 CDC16 CDK2 TIMELESS CDK1 ANAPC4 BIRC5 ANAPC5 ANAPC1 ANAPC2
87	1,10E-22	1,36E-20	38	239	M phase of mitotic cell cycle	ANAPC13 NCAPG CDA8 BUB1 IPKMYT1 ANAPC10 AURKB ANAPC11 AURKA CDC20 CCNB2 CCNB1 FZR1 CDC23 CDC27 NEK2 BUB1 TIPIN UBE2J ANAPC7 PLK1 CDC6 CDC25 NDC80 CCNA2 TPX2 CENPE CCNA1 CDC16 CDK2 TIMELESS CDK1 ANAPC4 BIRC5 ANAPC5 ANAPC1 ANAPC2
75	8,32E-21	6,55E-19	27	107	cell cycle checkpoint	BLM BUB1 BRIP1 CCNB1 FZR1 CDC45 CHEK1 RRBP8 NBN CLSPN HRAS BUB1 TIPIN TGFβ1 PLK1 H2AFX CDK6 CCNA2 CENPE MSH2 FAM175A CDK1 BIRC5 ATM TP53 ATR MAD2L1
7346	1,07E-11	3,66E-10	24	174	regulation of mitotic cell cycle	TGFβ1 PLK1 BUB1 B CDC6 CDC25C IPKMYT1 ANAPC10 EGFR CCNA2 TPX2 CENPE CCNB1 CDC23 CDC16 CDK2 CDK1 BIRC5 ATM NEK2 NBN TP53 HRAS BUB1 MAD2L1
10564	1,19E-08	2,53E-07	19	138	regulation of cell cycle process	TIPIN CREBBP TGFβ1 MRE11A CDC25C IPKMYT1 FOXO1 ANAPC10 TPX2 CENPE CCNB1 FZR1 CDC23 CDC16 TIMELESS BIRC5 ATM NEK2 BUB1
7093	3,57E-07	5,87E-06	12	52	mitotic cell cycle checkpoint	CCNA2 CENPE CCNB1 TGFβ1 CDK1 BUB1 B ATM NBN TP53 HRAS BUB1 MAD2L1
51327	1,15E-06	1,75E-05	15	102	M phase of meiotic cell cycle	H2AFX MRE11A MLH1 RAD51 B MSH6 CCNA1 RAD50 RAD51C RAD51 EXO1 CHEK1 CKS2 ATM NEK2 NBN
51329	1,15E-06	1,75E-05	15	102	interphase of mitotic cell cycle	BLM CUL5 CUL2 CDC6 CDC25C ANAPC10 EGFR PPP3CA CCNB1 CDC23 CDK2 AKT1 ANAPC4 BIRC5 ANAPC5 H2AFX MRE11A MLH1 RAD51 B MSH6 CCNA1 RAD50 RAD51C RAD51 EXO1 CHEK1 CKS2 ATM NEK2 NBN
51321	1,33E-06	1,99E-05	15	103	meiotic cell cycle	CDKN1A MCM7 NCAPG2 BUB1 B FOXO1 SMC4 SMC2 CKS1B CHEK1 EP300 AKT1 NEK2 TIPIN CDC25C SMC1A ICDC25A MSH6 CCNA2 CCNA1 DBF4 MSH2 FANCD2 TIMELESS MCM3 CKS2 BIRC5 MCM6 TP53 MCM2 NCAPG CDA8 IPKMYT1 NCAPH RNFB2 AURKB AURKA CCNB2 CCNB1 CDC45 MAPK1 CLSPN BUB1 IMAPK3 PLK1 FANCA ICDC7 CDC6 NDC80 TPX2 CENPE CDK2 CCNG1 MDM2 CDK1 ATM NCAPD2 NCAPD3 ATR MAD2L1
7049	4,53E-45	6,63E-42	59	794	cell cycle	CDKN1A NCAPG2 BUB1 B NCAPG CDA8 IPKMYT1 SMC4 NCAPH AURKB SMC2 AURKA CCNB2 CCNB1 CHEK1 AKT1 NEK2 BUB1 TIPIN PLK1 FANCA CDC7 CDC6 CDC25C SMC1A CDC25A NDC80 MSH6 CCNA2 TPX2 CCNA1 CENPE DBF4 FANCD2 CDK2 CCNG1 TIMELESS MCM2 CDK1 CKS2 BIRC5 ATM NCAPD2 NCAPD3 MAD2L1
22403	7,21E-37	5,27E-34	44	435	cell cycle phase	CDKN1A NCAPG2 BUB1 B NCAPG CDA8 IPKMYT1 SMC4 NCAPH AURKB SMC2 AURKA CCNB2 CCNB1 CHEK1 AKT1 NEK2 BUB1 TIPIN PLK1 FANCA CDC7 CDC6 CDC25C SMC1A CDC25A NDC80 MSH6 CCNA2 TPX2 CCNA1 CENPE DBF4 FANCD2 CDK2 CCNG1 TIMELESS MCM2 CDK1 CKS2 BIRC5 ATM NCAPD2 NCAPD3 MAD2L1
22402	5,73E-34	2,79E-31	46	582	cell cycle process	CDKN1A NCAPG2 BUB1 B NCAPG CDA8 IPKMYT1 SMC4 NCAPH AURKB SMC2 AURKA CCNB2 CCNB1 CHEK1 AKT1 NEK2 BUB1 TIPIN PLK1 FANCA CDC7 CDC6 CDC25C SMC1A CDC25A NDC80 MSH6 CCNA2 TPX2 CCNA1 CENPE DBF4 FANCD2 CDK2 CCNG1 TIMELESS MCM2 CDK1 CKS2 BIRC5 ATM NCAPD2 NCAPD3 MAD2L1
278	4,13E-32	1,21E-29	39	380	mitotic cell cycle	CDKN1A NCAPG2 BUB1 B NCAPG CDA8 IPKMYT1 SMC4 NCAPH AURKB SMC2 AURKA CCNB2 CCNB1 CHEK1 AKT1 NEK2 BUB1 TIPIN PLK1 FANCA CDC7 CDC6 CDC25C SMC1A CDC25A NDC80 MSH6 CCNA2 TPX2 CCNA1 CENPE DBF4 FANCD2 CDK2 CCNG1 TIMELESS MCM2 CDK1 CKS2 BIRC5 ATM NCAPD2 NCAPD3 MAD2L1
87	1,23E-30	3,01E-28	33	239	M phase of mitotic cell cycle	NCAPG2 BUB1 B NCAPG CDA8 IPKMYT1 SMC4 NCAPH AURKB SMC2 AURKA CCNB2 CCNB1 NEK2 BUB1 TIPIN PLK1 CDC6 CDC25C SMC1A CDC25A NDC80 CCNA2 TPX2 CCNA1 CENPE CDK2 CCNG1 TIMELESS CDK1 BIRC5 NCAPD2 NCAPD3 MAD2L1
51726	1,02E-26	1,36E-24	37	446	regulation of cell cycle	CDKN1A HDAC1 BUB1 B IPKMYT1 FOXO1 CKS1B CCNB1 CDC45 CHEK1 AKT1 NEK2 CLSPN BUB1 TIPIN JUN ICREBBP PLK1 CDC7 CDC6 CDC25C SMC1A CDC25A CCNA2 TPX2 CENPE MSH2 CDK2 CCNG1 TIMELESS MCM2 CDK1 CKS2 BIRC5 ATM TP53 ATR MAD2L1
75	2,29E-21	2,57E-19	21	107	cell cycle checkpoint	TIPIN CDKN1A PLK1 BUB1 B CDC6 SMC1A CCNA2 CENPE CCNB1 CDC45 MSH2 CHEK1 CCNG1 CDK1 BIRC5 ATM CLSPN TP53 BUB1 ATR MAD2L1
7346	2,52E-15	2,30E-13	20	174	regulation of mitotic cell cycle	CDKN1A PLK1 BUB1 B CDC6 CDC25C IPKMYT1 CCNA2 TPX2 CENPE CCNB1 CDK2 CCNG1 MCM2 CDK1 BIRC5 NEK2 ATM TP53 BUB1 MAD2L1
10564	4,70E-13	3,44E-11	17	138	regulation of cell cycle process	TIPIN CREBBP CDKN1A CDC7 CDC25C IPKMYT1 FOXO1 SMC1A TPX2 CENPE CCNB1 TIMELESS MCM2 BIRC5 NEK2 ATM BUB1
7093	4,22E-10	1,81E-08	11	52	mitotic cell cycle checkpoint	CCNA2 CENPE CCNB1 CDKN1A CCNG1 CDK1 BUB1 B ATM TP53 BUB1 MAD2L1
51329	9,39E-07	2,41E-05	11	102	interphase of mitotic cell cycle	CCNB1 CDKN1A DBF4 CDK2 MCM2 AKT1 BIRC5 CDC7 CDC6 CDC25C CDC25A

#: total number of nodes in the gene ontology (GO) annotation; *: number of nodes related to a given GO in the network.

Systemic effects of IEs in the cell cycle

This cluster (composed of clusters 2 and 4) addresses a particular area of interest in relation to whether metal ions and IEs interfere with other cellular responses to DNA damage, such as cell cycle progression and control. In clusters 2 and 4, AKT1, JUN and CREBBP and the TP53, CCNB1, CCNA2, CDK6, CDK2, CDK1, ATM, ATR, and CDK7 proteins were found to be bottlenecks together with Cr and S. The biological processes linked to this and its respective proteins are presented in Table 4.

Among all the chemical species present in coal mining environments, IEs, in particular, are capable of causing the most oxidative damage through the generation of ROS (Valko *et al.*, 2006). IEs can enter the body through inhalation or consumption of contaminated meals and then accumulate in the bloodstream (Schweinsberg and Von Karsa, 1990). These elements are deposited in tissues by various mechanisms (Bridges and Zalups, 2005) and may cause DNA damage. In this cluster, together with proteins regulated by oxidative stress and DNA damage, we also found proteins such as cyclins and cyclin-dependent kinases that have been reported to be down-regulated in response to ROS and are implicated in the induction of cell cycle arrest as one of the immediate defense mechanisms against genotoxic damage from oxidative stress (Burch and Heintz, 2005). Particularly, CCNB1 seems to be depleted in response to oxidative stress, causing the regulation of G2/M transit via the Chk1-Cdc2 DNA damage checkpoint pathway (Pyo *et al.*, 2013). Conversely, because altered cell cycle progression and/or cell cycle control and DNA repair inhibition have been observed under low, non-cytotoxic concentrations of metal compounds, some authors have suggested that inhibition could also be a result of the ability of metal ions to modify zinc finger proteins involved in cell cycle control and DNA repair (Hartwig *et al.*, 2002). Interestingly, some authors have reported the suppression of TP53-mediated cell cycle arrest in human breast cancer cells MCF7, as a response to DNA damage caused by Cd(II) (Méplan *et al.*, 1999). Other IEs involved in the modification of zinc finger proteins include Ni and Co (Hartwig and Schwerdtle, 2002). However, no similar implications have been reported for Cr and S.

As discussed in the previous section, Cr(VI) has been demonstrated to be consistently mutagenic in bacterial and mammalian model systems, and its carcinogenic activity is thought to be due to the induction of DNA damage generated by reactive intermediates, eventually resulting in DNA breakage (Vasylykiv *et al.*, 2010). Free radicals from SO₂ metabolism, such as SO₃⁻, SO₄⁻, SO₅⁻ may also induce DNA strand breaks (Meng *et al.*, 2005), and recent studies have confirmed that SO₂ derivatives (bisulfite and sulfite) cause mitotic delay in cultured human blood lymphocytes in a dose-dependent manner (Uren *et al.*, 2014).

Effect of El Cerrejón and Guacamaya coal exposure on alkaline and FPG high-throughput Comet assay

The results of the alkaline comet assay showed the presence of primary lesions (% DNA tail increase) in V79 cells exposed to ECCS (bituminous coal from El Cerrejón mine) and

Table 4 - Major cell cycle bioprocesses in clusters 2 and 4 associated with IEs.

GO ID	p-value	corr p-	k*	n [#]	Description	Genes in test set
278	6,09E-38	2,63E-36	60	380	mitotic cell cycle	CLTC BUB1 BPSMD8 CDC20 PSPMD9 PSPMD7 CDC23 PSPMD2 PSPMD3 CDC27 PSPMD1 AKT1 ANAPC7 RPS6 DNM2 PSPMA5 PMA6 PSPMA3 ADAMI7 PSPMA4 PSPMA1 PSPME3 PSPME1 RPL24 PSPME2 ANAPC4 ANAPC5 ANAPC1 ANAPC2 PSPMD10 ANAPC13 PSPMD12 PSPMD13 CUL2 ANAPC10 PSPMB10 ANAPC11 PSPMB6 PSPMB7 PSPMB4 CCNB1 FZR1 PSPMB5 PSPMB2 PSPMB3 PSPMB1 CLTCL1 PSPMB8 PSPMB9 MAD2L2 PSPMC6 PSPMC4 PSPMC1 CDC16 PSPMC2 MAD2L1
22402	4,93E-32	1,84E-30	65	582	cell cycle process	CLTC BUB1 BPSMD8 CDC20 PSPMD9 PSPMD7 CDC23 PSPMD2 PSPMD3 CDC27 PSPMD1 AKT1 ANAPC7 RPS6 DNM2 PSPMA5 PMA6 PSPMA3 ADAMI7 PSPMA4 PSPMA1 PSPME3 PSPME1 RPL24 PSPME2 ANAPC4 ANAPC5 ANAPC1 ANAPC13 PSPMD10 ANAPC13 PSPMD12 PSPMD13 CUL2 ANAPC10 PSPMB10 ANAPC11 PSPMB6 PSPMB7 PSPMB4 CCNB1 FZR1 PSPMB5 PSPMB2 PSPMB3 PSPMB1 CLTCL1 PSPMB8 PSPMB9 MAD2L2 PSPMC6 PSPMC4 PSPMC1 CDC16 PSPMC2 MAD2L1
7049	1,12E-25	3,45E-24	67	794	cell cycle	CLTC BUB1 BIRCA1 PSPMD8 CDC20 PSPMD9 PSPMD7 CDC23 PSPMD2 PSPMD3 CDC27 PSPMD1 AKT1 ANAPC7 RPS6 DNM2 PSPMA5 PMA6 PSPMA3 ADAMI7 PSPMA4 PSPMA1 PSPME3 PSPME1 RPL24 PSPME2 ANAPC4 ANAPC5 ANAPC1 ANAPC13 PSPMD10 ANAPC13 PSPMD12 PSPMD13 CUL2 ANAPC10 PSPMB10 ANAPC11 PSPMB6 PSPMB7 PSPMB4 CCNB1 FZR1 PSPMB5 PSPMB2 PSPMB3 PSPMB1 CLTCL1 PSPMB8 PSPMB9 MAD2L2 PSPMC6 PSPMC4 PSPMC1 CDC16 PSPMC2 MAD2L1
22403	3,84E-07	8,30E-06	30	435	cell cycle phase	ANAPC13 CUL5 CLTC CUL2 BUB1 ANAPC10 ANAPC11 CDC20 CCNB1 FZR1 CDC23 CDC27 CLTCL1 AKT1 ANAPC7 RPS6 DNM2 RAD51 B MAD2L2 ADAMI7 RAD51 CIRAD51 CDC16 MAD2L1 PSPMB10 ANAPC4 ANAPC5 ANAPC1 MAD2L1 ANAPC2
87	5,19E-06	1,03E-04	21	239	M phase of mitotic cell cycle	ANAPC13 ANAPC7 CLTC PSP6 BUB1 ANAPC10 ANAPC11 CDC20 MAD2L2 CCNB1 FZR1 CDC23 CDC27 CDC16 CLTCL1 RPL24 ANAPC4 ANAPC5 ANAPC1 MAD2L1 ANAPC2

Table 4 - cont.

7049	5,73E-35	4,37E-33	71	794	cell cycle	CCNK CDKN1A CCNT2 CCNT1 MCM7 CCNH CETN2 BUB1 BIRCA1 CKS1B CDC20 CDC23 EXO1 CHEK1 CDC27 EP300 NBN POLK POLE TIPIN LIG1 ANAPC7 LIG4 LIG3 RAD51B MSH6 CCNA2 CCNA1 RAD51C DBF4 MSH2 CKS2 TIMELESS MCM3 ANAPC4 ANAPC5 MCM6 TP53 ANAPC1 ANAPC2 MCM2 ANAPC13 BLM ANAPC10 ANAPC11 CCNB2 CCNB1 CDC45 POLD1 CLSPN BARD1 UBE2I UBE2B IRPA1 MRE11A CDC7 CDC6 MAD2L2 POLA1 RAD50 CDK6 RAD51 CDC16 CDK2 MDM2 CDK1 ATM MNAT1 ATR MAD2L1 TAF1
22403	2,64E-31	1,79E-29	53	435	cell cycle phase	CCNK CDKN1A CETN2 BUB1B CDC20 CDC23 EXO1 CHEK1 CDC27 NBN POLK POLE TIPIN ANAPC7 LIG3 RAD51B MSH6 CCNA2 CCNA1 RAD51C DBF4 CKS2 TIMELESS ANAPC4 ANAPC5 ANAPC1 ANAPC2 ANAPC13 BLM ANAPC10 ANAPC11 CCNB2 CCNB1 POLD1 BARD1 UBE2I UBE2B IRPA1 MRE11A CDC7 CDC6 MAD2L2 POLA1 RAD50 CDK6 RAD51 CDC16 CDK2 MDM2 CDK1 ATM MNAT1 MAD2L1 TAF1
22402	7,25E-28	4,15E-26	56	582	cell cycle process	CCNK CDKN1A CETN2 BUB1B CDC20 CDC23 EXO1 CHEK1 CDC27 NBN POLK POLE TIPIN ANAPC7 LIG3 RAD51B MSH6 CCNA2 CCNA1 RAD51C DBF4 MSH2 CKS2 TIMELESS ANAPC4 ANAPC5 ANAPC1 ANAPC2 ANAPC13 BLM ANAPC10 ANAPC11 CCNB2 CCNB1 POLD1 BARD1 UBE2I UBE2B IRPA1 MRE11A CDC7 CDC6 MAD2L2 POLA1 RAD50 CDK6 RAD51 CDC16 CDK2 MDM2 CDK1 ATM MNAT1 MAD2L1 TAF1
51726	1,75E-27	9,46E-26	50	446	regulation of cell cycle	CCNK CDKN1A CCNT2 CCNT1 BUB1B BIRCA1 CKS1B CCND3 CDC23 CASP3 CHEK1 NBN TIPIN DDB1 CCNA2 MSH2 CKS2 TIMELESS TP53 ANAPC2 BLM ANAPC10 BRIP1 CCNB1 CDC45 RBBP8 CLSPN BARD1 JUN CREBBP UBE2B MRE11A CDC7 GTSE1 F2H1 CDC6 MAD2L2 CDK7 COP5 CDK6 ERCC3 CDC16 FAM175A CDK2 ERCC2 MDM2 CDK1 ATM MNAT1 ATR MAD2L1
75	5,24E-20	2,13E-18	25	107	cell cycle checkpoint	CDKN1A BLM BUB1 BIRCA1 BRIP1 CCNB1 CDC45 CHEK1 RBBP8 NBN CLSPN TIPIN CDC6 DDB1 MAD2L2 CCNA2 MSH2 ERCC3 FAM175A ERCC2 CDK1 ATM TP53 ATR MAD2L1
278	4,71E-19	1,88E-17	39	380	mitotic cell cycle	ANAPC13 CCNK CDKN1A BLM CETN2 BUB1B ANAPC10 ANAPC11 CDC20 CCNB2 CCNB1 CDC23 POLD1 CDC27 POLK POLK POLE TIPIN UBE2I ANAPC7 CDC7 CDC6 MAD2L2 CCNA2 POLA1 CCNA1 CDK6 DBF4 CDC16 CDK2 TIMELESS MDM2 CDK1 ANAPC4 ANAPC5 MNAT1 ANAPC1 MAD2L1 ANAPC2 TAF1
87	3,12E-14	1,00E-12	28	239	M phase of mitotic cell cycle	ANAPC13 CCNK CETN2 BUB1B ANAPC10 ANAPC11 CDC20 CCNB2 CCNB1 CDC23 CDC27 POLK TIPIN UBE2I ANAPC7 CDC6 MAD2L2 CCNA2 CCNA1 CDC16 CDK2 TIMELESS CDK1 ANAPC4 ANAPC5 ANAPC1 MAD2L1 ANAPC2
51329	2,90E-11	6,99E-10	18	102	interphase of mitotic cell cycle	CDKN1A BLM CDC7 CDC6 ANAPC10 POLA1 CCNB1 CDC23 CDK6 DBF4 POLD1 CDK2 MDM2 ANAPC4 ANAPC5 MNAT1 POLK POLE TAF1
51327	1,02E-07	1,44E-06	15	102	M phase of meiotic cell cycle	UBE2B IRPA1 MRE11A LIG3 RAD51B MSH6 CCNA1 RAD50 RAD51C RAD51 EXO1 CHEK1 CKS2 ATM NBN
51321	1,18E-07	1,65E-06	15	103	meiotic cell cycle	UBE2B IRPA1 MRE11A LIG3 RAD51B MSH6 CCNA1 RAD50 RAD51C RAD51 EXO1 CHEK1 CKS2 ATM NBN
10564	8,19E-06	9,75E-05	15	138	regulation of cell cycle process	TIPIN CREBBP CDKN1A UBE2B MRE11A CDC7 BIRCA1 ANAPC10 MAD2L2 CCNB1 CDC23 CDC16 TIMELESS MDM2 ATM MNAT1 ATR MAD2L1 TAF1
7093	2,08E-05	2,38E-04	10	52	mitotic cell cycle checkpoint	MAD2L2 CCNA2 CDKN1A CCNB1 CDK1 BUB1B ATM NBN TP53 MAD2L1
7346	2,63E-05	2,95E-04	16	174	regulation of mitotic cell cycle	CDKN1A BUB1B CDC6 ANAPC10 MAD2L2 CCNA2 CCNB1 CDC23 CDC16 CDK2 MDM2 CDK1 ATM NBN TP53 MAD2L1
86	9,00E-05	9,82E-04	7	21	G2/M transition of mitotic cell cycle	CDKN1A CCNB1 CDK2 ANAPC4 ANAPC5 ANAPC10 TAF1

#: total number of nodes in the gene ontology (GO) annotation; *: number of nodes related to a given GO in the netwo

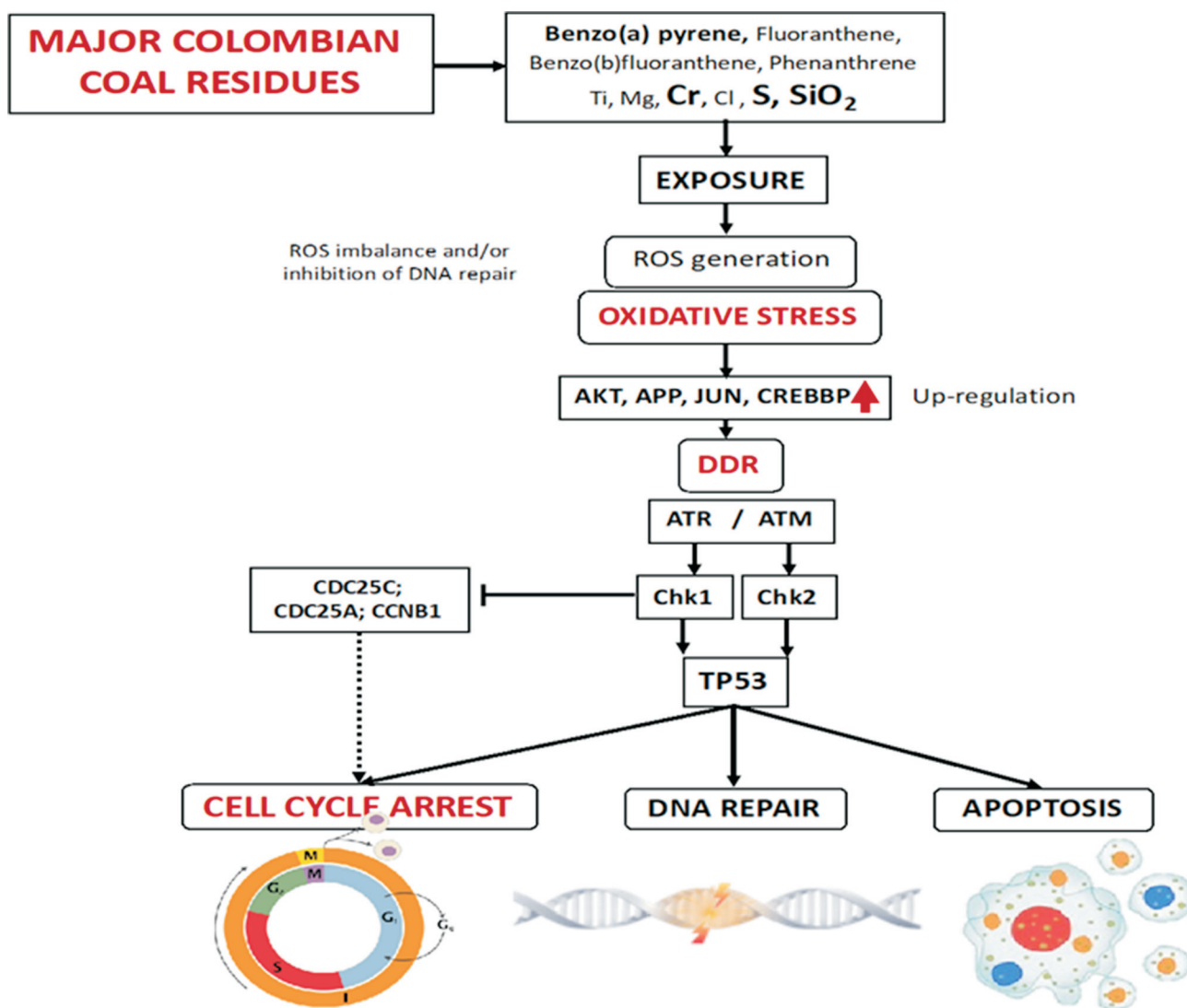


Figure 11 - Molecular model illustrating how major coal residues potentially affect cell cycle progression: Exposure to major coal residues, such as benzo[a]pyrene, fluoranthene, benzo[b]fluoranthene, phenanthrene, Ti, Mg, Cr, Cl, S, and SiO₂, can generate ROS via several pathways (e.g., Fenton-like reactions). The ROS imbalance and/or inhibition of the DNA repair process can lead to oxidative stress and the upregulation of several proteins associated with the oxidative response (AKT, APP, JUN and CREBBP) which are also involved in the control of the cell cycle. DNA and protein damage caused by the oxidative damage triggers DNA damage response mechanisms (DDR), including the protein kinase cascades ATM-Chk2/ATR-Chk1, which may result in cell cycle arrest. Oxidative stress can also induce cell cycle arrest through the degradation of CDC25C via the Chk1 protein kinase-dependent pathway. ATR phosphorylates and activates Chk1, which in turn, phosphorylates and inhibits Cdc25 phosphatases. Cdc25 inhibition ends up causing cell cycle arrest. Cdc25A phosphorylation by Chk1 triggers its degradation in a ubiquitin/proteasome-dependent manner. Both kinases phosphorylate TP53. In response to DNA damage, the activation of TP53 activates the expression of numerous genes involved in cell cycle arrest, DNA repair, apoptosis, and many other processes.

LGCS (sub-bituminous coal from La Guacamaya mine) for 24 h. Additionally, the results of the modified comet assay show that the cultures exposed to ECCS maintain the same levels of % tail DNA, whereas the cultures exposed to LGCS showed an increase in % tail DNA, when compared to the no-enzyme groups. These results could indicate oxidative damage. Previous studies on coal and its products demonstrated resulting DNA damage and oxidative stress induced by the presence of IE and PAH (Valko *et al.*, 2006; da Silva, 2016). Such results may also be due to compounds identified in the current study, in which we report various levels of inorganic elements (heavy metals) in the bituminous coal from ECCS and sub-bituminous coal from LGCS and high levels of chromium in the coal from LGCS. It

was known that some IEs (heavy metals) could generate oxidative damage by generating ROS (Valko *et al.*, 2006). Multiple cellular processes including cell cycle checkpoint activation and DNA repair are typically initiated in response to such DNA damage (Dasika *et al.*, 1999; Lima *et al.*, 2016).

Conclusions

Using a systems chemo-biology approach, we examined how some of the major chemical constituents of coal dust and PM derived from coal mining activities interact with specific biological processes relation to the cell cycle. The main proteins and compounds present in the network were taken into

account to construct a molecular model characterizing the effects of major coal residues on the cell cycle (Figure 11). The analysis performed in the present study suggests that coal residue MIOs (SiO₂), IEs (Ti, Mg, Cr, Cl and S) and PAHs (benzo[a]pyrene, fluoranthene, benzo[b]fluoranthene and phenanthrene) can generate ROS. The resultant oxidative stress can induce cell cycle arrest through the upregulation of proteins such as AKT, APP, JUN and CREBBP, leading to DNA damage response activation by ATM/ATR and Chk1/Chk2 or by CDC25C or CCNB1 degradation. The model also suggested that protein p53 could be activated by Chk1/Chk2 and induce cell cycle arrest, senescence or apoptosis.

Acknowledgments

This work was supported by a grant from Conselho Nacional para o Desenvolvimento Científico e Tecnológico-CNPq, Brazil; Universal Grant Number 454288/2014-0.

Conflict of interest

The authors declare no conflict of interest.

Author's contribution

JFTA, JS, and JAPH proposed and conceived the analysis. LFOS conducted the experiments to identify the major inorganic oxides in coal ashes. JFD conducted the experiments on IEs measurements in the particle-induced X-ray emission (PIXE) assay. DSC conducted the analyses of measurements and quantification of polycyclic aromatic hydrocarbons. JFTA and LEP conducted the experiments in the modified alkaline comet assay. JFTA, LEP, DB, and FRS constructed the networks, analyzed, and interpreted the data. JFTA and LEP wrote the manuscript with support from DB. IMO contributed to the final version of the paper. All authors discussed the results and contributed to editing the final manuscript.

REFERENCES

- Alfaro-Moreno E, Martínez L, García-Cuellar C, Bonner JC, Murray JC, Rosas I, Rosales SP and Osornio-Vargas AR (2002) Biologic effects induced in vitro by PM10 from three different zones of Mexico City. *Environ Health Persp* 110:715-720.
- Asweto CO, Wu J, Hu H, Feng L, Yang X, Duan J and Sun Z (2017) Combined Effect of Silica Nanoparticles and Benzo[a]pyrene on Cell Cycle Arrest Induction and Apoptosis in Human Umbilical Vein Endothelial Cells. *Int J Environ Res Public Health* 14:289.
- Azevedo H and Moreira-Filho CA (2015) Topological robustness analysis of protein interaction networks reveals key targets for overcoming chemotherapy resistance in glioma. *Sci Rep-UK* 5:16830.
- Bader GD and Hogue CW (2003) An automated method for finding molecular complexes in large protein interaction networks. *BMC Bioinformatics* 4:2.
- Benjamini Y and Hochberg Y (1995) Controlling the false discovery rate: a practical and powerful approach to multiple testing. *J Roy Stat Soc B Met* 57:289-300.
- Bianchi M, Giacomini E, Crinelli R, Radici L, Carloni E and Magnani M (2015) Dynamic transcription of ubiquitin genes under basal and stressful conditions and new insights into the multiple UBC transcript variants. *Gene* 573:100-109.
- Billet S, Abbas I, Le Goff J, Verdin A, Andre V, Lafargue PE, Hachimi A, Cazier F, Sichel F, Shirali P and Garcon G (2008) Genotoxic potential of Polycyclic Aromatic Hydrocarbons-coated onto airborne Particulate Matter (PM 2.5) in human lung epithelial A549 cells. *Cancer Lett* 270:144-155.
- Blissett RS and Rowson NA (2012) A review of the multi-component utilisation of coal fly ash. *Fuel* 97:1-23.
- Borm PJ (1997) Toxicity and occupational health hazards of coal fly ash (CFA). A review of data and comparison to coal mine dust. *Ann Occup Hyg* 41:659-676.
- British Petroleum (2014) BP Statistical Review of World Energy. British Petroleum, London.
- Branzei D and Foiani M (2008) Regulation of DNA repair throughout the cell cycle. *Nat Rev Mol Cell Bio* 9:297-308.
- Bridges CC and Zalups RK (2005) Molecular and ionic mimicry and the transport of toxic metals. *Toxicol Appl Pharmacol* 204:274-308.
- Brook RD, Rajagopalan S, Pope CA 3rd, Brook JR, Bhatnagar A, Diez-Roux AV, Holguin F, Hong Y, Luepker RV, Mittleman MA *et al.* (2010) Particulate matter air pollution and cardiovascular disease: An update to the scientific statement from the American Heart Association. *Circulation* 121:2331-2378.
- Burch PM and Heintz NH (2005) Redox regulation of cell-cycle re-entry: cyclin D1 as a primary target for the mitogenic effects of reactive oxygen and nitrogen species. *Antioxid Redox Signal* 7:741-751.
- Callen MS, de la Cruz MT, Lopez JM, Navarro MV and Mastral AM (2009) Comparison of receptor models for source apportionment of the PM10 in Zaragoza (Spain). *Chemosphere* 76:1120-1129.
- Campbell JL, Boyd NI, Grassi N, Bonnick P and Maxwell JA (2010) The Guelph PIXE software package IV. *Nucl Instrum Meth B* 268:3356-3363.
- Cavalcante RM, de Lima DM, Correia LM, Nascimento RF, Silveira ER, Freire GS and Viana RB (2008) Técnicas de extrações e procedimentos de clean-up para a determinação de hidrocarbonetos policíclicos aromáticos (HPA) em sedimentos da costa do Ceará. *Quím Nova* 31:1371-1377.
- Celik M, Donbak L, Unal F, Yuzbasioglu D, Aksoy H and Yilmaz S (2007) Cytogenetic damage in workers from a coal-fired power plant. *Mutat Res* 627:158-163.
- Chaulya S (2004) Assessment and management of air quality for an opencast coal mining area. *J Environ Manage* 70:1-14.
- Chiang HC and Tsou TC (2009) Arsenite enhances the benzo[a]pyrene diol epoxide (BPDE)-induced mutagenesis with no marked effect on repair of BPDE-DNA adducts in human lung cells. *Toxicol In Vitro* 23:897-905.
- Chiba S, Okayasu K, Tsuchiya K, Tamaoka M, Miyazaki Y, Inase N and Sumi Y (2017) The C-jun N-terminal kinase signaling pathway regulates cyclin D1 and cell cycle progression in airway smooth muscle cell proliferation. *Int J Clin Exp Med* 10:2252-2262.
- Choi WJ, Banerjee J, Falcone T, Bena J, Agarwal A and Sharma RK (2007) Oxidative stress and tumor necrosis factor-alpha-induced alterations in metaphase II mouse oocyte spindle structure. *Fertil Steril* 88:1220-1231.
- Collins AR (2009) Investigating oxidative DNA damage and its repair using the comet assay. *Mut Res* 681:24-32.
- D'Angiolella V, Santarpia C and Grieco D (2007) Oxidative stress overrides the spindle checkpoint. *Cell Cycle* 6:576-579.

- da Silva J (2016) DNA damage induced by occupational and environmental exposure to miscellaneous chemicals. *Mutat Res* 770:170-182.
- Dasika GK, Lin SCJ, Zhao S, Sung P, Tomkinson A and Lee EY (1999) DNA damage-induced cell cycle checkpoints and DNA strand break repair in development and tumorigenesis. *Oncog* 18:7883-7899.
- de Kok TM, Hogervorst JG, Briede JJ, van Herwijnen MH, Maas LM, Moonen EJ, Drieste HA and Kleinjans JC (2005) Genotoxicity and physicochemical characteristics of traffic-related ambient particulate matter. *Environ Mol Mutagen* 46:71-80.
- Espitia-Pérez L, da Silva J, Espitia-Pérez P, Brango H, Salcedo-Arteaga S, Hoyos-Giraldo LS, de Souza CT, Dias JF, Agudelo-Castañeda D, Valdés Toscano A *et al.* (2018) Cytogenetic instability in populations with residential proximity to open-pit coal mine in Northern Colombia in relation to PM10 and PM2.5 levels. *Ecotox and Environ Saf* 148:453-466.
- Feltes BC, de Faria Poloni J, Notari DL and Bonatto D (2013) Toxicological Effects of the Different Substances in Tobacco Smoke on Human Embryonic Development by a Systems Chemo-Biology Approach. *PLoS ONE* 8:e61743.
- Feng B, Jensen A, Bhatia SK and Dam-Johansen K (2003) Activation energy distribution of thermal annealing of a bituminous coal. *Energ Fuel* 17:399-404.
- Fischer JM, Robbins SB, Al-Zoughool M, Kannamkumarath SS, Stringer SL, Larson JS, Caruso JA, Talaska G, Stambrook PJ and Stringer JR (2005) Co-mutagenic activity of arsenic and benzo[a]pyrene in mouse skin. *Mutat Res* 588:35-46.
- Gauthier PT, Norwood WP, Prepas EE and Pyle GG (2015) Metal-polycyclic aromatic hydrocarbon mixture toxicity in *Hyalomma azteca*. 2. Metal accumulation and oxidative stress as interactive co-toxic mechanisms. *Environ Sci Technol* 49:11780-11788.
- Gloscow EJ (2007) *New Research on Genomic Instability*. Nova Science Publishers, Nova York.
- Gualtieri M, Øvrevik J, Møllerup S, Asare N, Longhin E, Dahlman HJ, Camatini M and Holme JA (2011) Airborne urban particles (Milan winter-PM 2.5) cause mitotic arrest and cell death: effects on DNA, mitochondria, AhR binding and spindle organization. *Mutat Res* 713:18-31.
- Gutzkow KB, Langleite TM, Meier S, Graupner A, Collins AR and Brunborg G (2013) High-throughput comet assay using 96 minigels. *Mutagen* 28:333-40.
- Hartwig A, Asmuss M, Ehleben I, Herzer U, Kostelac D, Pelzer A, Schwerdtle T and Bürkle A (2002) Interference by toxic metal ions with DNA repair processes and cell cycle control: molecular mechanisms. *Environ Health Perspect* 110 Suppl 5:797-799.
- Hartwig A and Schwerdtle T (2002) Interactions by carcinogenic metal compounds with DNA repair processes: toxicological implications. *Toxicol Lett* 127:47-54.
- Hsiao WL, Mo ZY, Fang M, Shi XM and Wang F (2000) Cytotoxicity of PM(2.5) and PM(2.5-10) ambient air pollutants assessed by the MTT and the Comet assays. *Mutat Res* 471:45-55.
- Huang YC, Rappold AG, Graff DW, Ghio AJ and Devlin RB (2012) Synergistic effects of exposure to concentrated ambient fine pollution particles and nitrogen dioxide in humans. *Inhal Toxicol* 24:790-797.
- Huertas JI, Huertas ME, Izquierdo S and González ED (2012a) Air quality impact assessment of multiple open pit coal mines in northern Colombia. *J Environ Manage* 93:121-129.
- Huertas JI, Huertas ME and Solis DA (2012b) Characterization of airborne particles in an open pit mining region. *Sci Total Environ* 423:39-46.
- Jensen LJ, Kuhn M, Stark M, Chaffron S, Creevey C, Muller J, Doerks T, Julien P, Roth A, Simonovic M *et al.* (2009) STRING 8—a global view on proteins and their functional interactions in 630 organisms. *Nucleic Acids Res* 37:D412-416.
- Johansson SAE, Campbell JL and Malmqvist KG (1995) *Particle-Induced X-Ray Emission Spectrometry (PIXE)*. Wiley-Blackwell, Hoboken.
- Kim SM, Lee HM, Hwang KA and Choi KC (2017) Benzo(a)pyrene induced cell cycle arrest and apoptosis in human chorioncarcinoma cancer cells through reactive oxygen species-induced endoplasmic reticulum-stress pathway. *Food Chem Toxicol* 107:339-348.
- Kiskinis E, Suter W and Hartmann A (2002) High throughput comet assay using 96-well plates. *Mutagen* 17:37-43.
- Klein JA and Ackerman SL (2003) Oxidative stress, cell cycle, and neurodegeneration. *J Clin Invest* 111:785-793.
- Kocbach A, Herseth JI, Låg M, Refsnes M and Schwarze PE (2008) Particles from wood smoke and traffic induce differential pro-inflammatory response patterns in co-cultures. *Toxicol Appl Pharmacol* 232:317-326.
- Kothai P, Prathibha P, Saradhi I, Pandit G and Puranik V (2009) Characterization of atmospheric particulate matter using pixe technique. *Int J Environ Sci Eng* 3:39-42.
- Ku T, Chen M, Li B, Yun Y, Li G and Sang N (2017) Synergistic effects of particulate matter (PM 2.5) and sulfur dioxide (SO 2) on neurodegeneration via the microRNA-mediated regulation of tau phosphorylation. *Toxicol Res (Camb)* 6:7-16.
- Kushwaha S, Vikram A, Trivedi PP and Jena GB (2011) Alkaline, Endo III and FPG modified comet assay as biomarkers for the detection of oxidative DNA damage in rats with experimentally induced diabetes. *Mutat Res* 726:242-250.
- Labranche N, El Khattabi C, Dewachter L, Dreyfuss C, Fontaine J, Van De Borne P, Berkenboom G and Pochet S (2012) Vascular oxidative stress induced by diesel exhaust microparticles: synergism with hypertension. *J Cardiovasc Pharmacol* 60:530-537.
- Lee D and Ryu KY (2017) Effect of cellular ubiquitin levels on the regulation of oxidative stress response and proteasome function via Nrf1. *Biochem Biophys Res Commun* 485:234-240.
- Leon-Mejia G, Espitia-Perez L, Hoyos-Giraldo LS, da Silva J, Hartmann A, Henriques JA and Quintana M (2011) Assessment of DNA damage in coal open-cast mining workers using the cytokinesis-blocked micronucleus test and the comet assay. *Sci Total Environ* 409:686-691.
- Leon-Mejia G, Silva LF, Civeira MS, Oliveira ML, Machado M, Villela IV, Hartmann A, Premoli S, Correa DS, da Silva J *et al.* (2016) Cytotoxicity and genotoxicity induced by coal and coal fly ash particles samples in V79 cells. *Environ Sci Pollut Res Int* 23:24019-24031.
- Lin MT and Beal MF (2006) Mitochondrial dysfunction and oxidative stress in neurodegenerative diseases. *Nature* 443:787-795.
- Lima M, Bouzid H, Soares DG, Selle F, Morel C, Galmarini CM, Henriques JAP, Larsen AK and Escargueil AE (2016) Dual inhibition of ATR and ATM potentiates the activity of trabectedin and lurbectedin by perturbing the DNA damage response and homologous recombination repair. *Oncotarget* 7:25885-25901.
- Liu G, Niu Z, Van Niekerk D, Xue J and Zheng L (2008) Polycyclic aromatic hydrocarbons (PAHs) from coal combustion: emissions, analysis, and toxicology. *Rev Environ Contam Toxicol* 192:1-28.
- Longhin E, Holme JA, Gutzkow KB, Arlt VM, Kucab JE, Camatini M and Gualtieri M (2013) Cell cycle alterations induced by urban PM2.5 in bronchial epithelial cells: characterization of

- the process and possible mechanisms involved. *Part Fibre Toxicol* 10:63.
- McNamee J (2000) Comet assay: rapid processing of multiple samples. *Mutat Res Toxicol Environ Mutagen* 466:63–9.
- Maere S, Heymans K and Kuiper M (2005) BiNGO: a Cytoscape plugin to assess overrepresentation of gene ontology categories in biological networks. *Bioinformatics* 21:3448–3449.
- Meixner A, Karreth F, Kenner L, Penninger JM and Wagner EF (2010) Jun and JunD-dependent functions in cell proliferation and stress response. *Cell Death Differ* 17:1409–1419.
- Meng Z, Qin G and Zhang B (2005) DNA damage in mice treated with sulfur dioxide by inhalation. *Environ Mol Mutagen* 46:150–155.
- Meplan C, Mann K and Hainaut P (1999) Cadmium induces conformational modifications of wild-type p53 and suppresses p53 response to DNA damage in cultured cells. *J Biol Chem* 274:31663–31670.
- Mouton-Liger F, Paquet C, Dumurgier J, Bouras C, Pradier L, Gray F and Hugon J (2012) Oxidative stress increases BACE1 protein levels through activation of the PKR-eIF2 α pathway. *Biochim Biophys Acta* 1822:885–896.
- Muche A, Arendt T and Schliebs R (2017) Oxidative stress affects processing of amyloid precursor protein in vascular endothelial cells. *PLoS One* 12:e0178127.
- Muthusamy S, Peng C and Ng JC (2018) Genotoxicity evaluation of multi-component mixtures of polyaromatic hydrocarbons (PAHs), arsenic, cadmium, and lead using flow cytometry based micronucleus test in HepG2 cells. *Mutat Res Genet Toxicol Environ Mutagen* 827:9–18.
- Nathan C and Cunningham-Bussell A (2013) Beyond oxidative stress: an immunologist's guide to reactive oxygen species. *Nat Rev Immunol* 13:349–361.
- Nathan Y, Dvorachek M, Pelly I and Mimran U (1999) Characterization of coal fly ash from Israel. *Fuel* 78:205–213.
- Norrish K and Hutton JT (1969) An accurate X-ray spectrographic method for the analysis of a wide range of geological samples. *Geochim Cosmochim Acta* 33:431–453.
- Otto T and Sicinski P (2017) Cell cycle proteins as promising targets in cancer therapy. *Nat Rev Cancer* 17:93–115.
- Pandey B, Agrawal M and Singh S (2014) Assessment of air pollution around coal mining area: Emphasizing on spatial distributions, seasonal variations and heavy metals, using cluster and principal component analysis. *Atmospheric Pollution Research* 5:79–86.
- Parker AL, Kavallaris M and McCarroll JA (2014) Microtubules and their role in cellular stress in cancer. *Front Oncol* 4:153.
- Pearce AK and Humphrey TC (2001) Integrating stress-response and cell-cycle checkpoint pathways. *Trends Cell Biol* 11:426–433.
- Peng C, Muthusamy S, Xia Q, Lal V, Denison MS and Ng JC (2015) Micronucleus formation by single and mixed heavy metals/loids and PAH compounds in HepG2 cells. *Mutagen* 30:593–602.
- Poma A, Limongi T, Pisani C, Granato V and Picozzi P (2006) Genotoxicity induced by fine urban air particulate matter in the macrophages cell line RAW 264.7. *Toxicol In Vitro* 20:1023–1029.
- Pope CA 3rd, Burnett RT, Thun MJ, Calle EE, Krewski D, Ito K and Thurston GD (2002) Lung cancer, cardiopulmonary mortality, and long-term exposure to fine particulate air pollution. *Jama* 287:1132–1141.
- Pope CA 3rd, Burnett RT, Turner MC, Cohen A, Krewski D, Jerrett M, Gapstur SM and Thun MJ (2011) Lung cancer and cardiovascular disease mortality associated with ambient air pollution and cigarette smoke: shape of the exposure-response relationships. *Environ Health Perspect* 119:1616–1621.
- Pope CA and Dockery DW (2006) Health effects of fine particulate air pollution: lines that connect. *J Air Waste Manag Assoc* 56:709–742.
- Prada-Fonseca M, Caicedo-Pineda G and Márquez-Godoy M (2016) Comparación del potencial oxidativo de *Acidithiobacillus ferrooxidans*, en un proceso de biodesulfurización de carbón. *Rev Colomb Biotecnol* 18:57–64.
- Puente BN, Kimura W, Muralidhar SA, Moon J, Amatruda JF, Phelps KL, Grinsfelder D, Rothermel BA, Chen R, Garcia JA *et al.* (2014) The oxygen-rich postnatal environment induces cardiomyocyte cell-cycle arrest through DNA damage response. *Cell* 157:565–579.
- Pyo CW, Choi JH, Oh SM and Choi SY (2013) Oxidative stress-induced cyclin D1 depletion and its role in cell cycle processing. *Biochim Biophys Acta* 1830:5316–5325.
- Rebhan M, Chalifa-Caspi V, Prilusky J and Lancet D (1997) GeneCards: integrating information about genes, proteins and diseases. *Trends Genet* 13:163.
- Rieder CL (2011) Mitosis in vertebrates: the G2/M and M/A transitions and their associated checkpoints. *Chromosome Res* 19:291–306.
- Safran M, Dalah I, Alexander J, Rosen N, Iny Stein T, Shmoish M, Nativ N, Bahir I, Doniger T, Krug H *et al.* (2010) GeneCards Version 3: the human gene integrator. *Database (Oxford)* 2010:baq020.
- Sambandam B, Devasena T, Islam VI and Prakhya BM (2015) Characterization of coal fly ash nanoparticles and their induced in vitro cellular toxicity and oxidative DNA damage in different cell lines. *Indian J Exp Biol* 53:585–593.
- Savitsky PA and Finkel T (2002) Redox regulation of Cdc25C. *Int J Biol Chem* 277:20535–20540.
- Scardoni G, Pettegiani M and Laudanna C (2009) Analyzing biological network parameters with CentiScaPe. *Bioinformatics* 25:2857–2859.
- Schins RP and Borm PJ (1999) Mechanisms and mediators in coal dust induced toxicity: a review. *Ann Occup Hyg* 43:7–33.
- Schreiber M, Kolbus A, Piu F, Szabowski A, Möhle-Steinlein U, Tian J, Karin M, Angel P and Wagner EF (1999) Control of cell cycle progression by c-Jun is p53 dependent. *Genes Dev* 13:607–619.
- Schweinsberg F and von Karsa L (1990) Heavy metal concentrations in humans. *Comp Biochem Physiol C* 95:117–123.
- Scott J (2017) *Social Network Analysis*. SAGE Publications, Nova York.
- Shannon P, Markiel A, Ozier O, Baliga NS, Wang JT, Ramage D, Amin N, Schwikowski B and Ideker T (2003) Cytoscape: a software environment for integrated models of biomolecular interaction networks. *Genome Res* 13:2498–2504.
- Singh NP, McCoy MT, Tice R and Schneider EL (1988) A simple technique for quantitation of low levels of DNA damage in individual cells. *Exp Cell Res* 175:184–91.
- Snel B, Lehmann G, Bork P and Huynen MA (2000) STRING: a web-server to retrieve and display the repeatedly occurring neighbourhood of a gene. *Nucleic Acids Res* 28:3442–3444.
- Sun F, Littlejohn D and Gibson MD (1998) Ultrasonication extraction and solid phase extraction clean-up for determination of US EPA 16 priority pollutant polycyclic aromatic hydrocarbons in soils by reversed-phase liquid chromatography with ultraviolet absorption detection. *Anal Chim Acta* 364:1–11.
- Tice R, Agurell E, Anderson D, Burlinson B, Hartmann A, Kobayashi H, Miyamae Y, Rojas E, Ryu JC and Sasaki YF (2000) Single-cell gel/comet assay: guidelines for in vitro and in vivo genetic toxicology testing. *Env Mol Mutagen* 35:206–21.

- Tran HP, Prakash AS, Barnard R, Chiswell B and Ng JC (2002) Arsenic inhibits the repair of DNA damage induced by benzo(a)pyrene. *Toxicol Lett* 133:59-67.
- Tucker JD and Ong TM (1985) Induction of sister chromatid exchanges by coal dust and tobacco snuff extracts in human peripheral lymphocytes. *Environ Mutagen* 7:313-324.
- Uren N, Yuksel S and Onal Y (2014) Genotoxic effects of sulfur dioxide in human lymphocytes. *Toxicol Ind Health* 30:311-315.
- Valko M, Rhodes CJ, Moncol J, Izakovic M and Mazur M (2006) Free radicals, metals and antioxidants in oxidative stress-induced cancer. *Chem Biol Interact* 160:1-40.
- Vasylykiv OY, Kubrak OI, Storey KB and Lushchak VI (2010) Cytotoxicity of chromium ions may be connected with induction of oxidative stress. *Chemosphere* 80:1044-1049.
- Wang X, McCullough KD, Franke TF and Holbrook NJ (2000) Epidermal growth factor receptor-dependent Akt activation by oxidative stress enhances cell survival. *J Biol Chem* 275:14624-14631.
- Wise SS and Wise JP (2010) Aneuploidy as an early mechanistic event in metal carcinogenesis. *Biochem Soc Trans* 38:1650-1654.

Supplementary Material:

The following online material is available for this article:

[Figure S1](#) - Coal sample collection sites in Colombia.

[Figure S2](#) - Main CPI-PPI network generated by the Cytoscape 3.4.0 program.

[Table S1](#) - Major inorganic oxide components in coal ashes (%wt) as identified by XRF.

[Table S2](#) - IEs concentrations in coal samples as revealed by the PIXE assay (mean \pm standard deviation).

[Table S3](#) - Polycyclic aromatic hydrocarbon concentrations per sample (mean \pm standard deviation) as revealed by HPLC/UV/Vis.

[Table S4](#) - Proteins involved in hub-bottlenecks (HBs) and their function.

Associate Editor: Regina C. Mingroni-Netto

License information: This is an open-access article distributed under the terms of the Creative Commons Attribution License (type CC-BY), which permits unrestricted use, distribution and reproduction in any medium, provided the original article is properly cited.